3-13-2017

Synthesis and Characterization of Well-Defined PEGylated Polypeptoids as Protein-Resistant Polymers

Sunting Xuan
Macromolecular Studies Group

Sudipta Gupta
Macromolecular Studies Group

Xin Li
Macromolecular Studies Group

Markus Bleuel
National Institute of Standards and Technology

Gerald J. Schneider
Macromolecular Studies Group

See next page for additional authors

Recommended Citation

Xuan, S., Gupta, S., Li, X., Bleuel, M., Schneider, G., & Zhang, D. (2017). Synthesis and Characterization of Well-Defined PEGylated Polypeptoids as Protein-Resistant Polymers. *Biomacromolecules, 18* (3), 951-964. https://doi.org/10.1021/acs.biomac.6b01824

Article

Synthesis and Characterization of Well-defined PEGylated Polypeptoids as Protein-resistant Polymers

Sunting Xuan, Sudipta Gupta, Xin Li, Markus Bleuel, Gerald J. Schneider, and Donghui Zhang

Biomacromolecules, **Just Accepted Manuscript** • DOI: 10.1021/acs.biomac.6b01824 • Publication Date (Web): 06 Feb 2017

Synthesis and Characterization of Well-defined PEGylated Polypeptoids as Protein-resistant Polymers

Sunting Xuan,[1] Sudipta Gupta,[1] Xin Li,[1] Markus Bleuel,[3] Gerald J. Schneider[1,2*] and Donghui Zhang[1*]

[1]*Department of Chemistry and Macromolecular Studies Group, Louisiana State University, Baton Rouge, LA 70803, USA*

[2]*Department of Physics, Louisiana State University, Baton Rouge, LA 70803, USA*

[3]*NIST Center for Neutron Research, National Institute of Standards and Technology, Gaithersburg, Maryland 20899, United States*

*Corresponds to: dhzhang@lsu.edu and gjschneider@lsu.edu

ABSTRACT: Well-defined polypeptoids bearing oligomeric ethylene glycol side chains PNMe(OEt)$_n$G (n = 1-3) with controlled molecular weight (3.26-28.6 kg/mol) and narrow molecular distribution (polydispersity index, PDI = 1.03-1.10) have been synthesized by ring-opening polymerization of the corresponding *N*-carboxyanhydrides having oligomeric ethylene glycol side chains (Me(OEt)$_n$-NCA, n = 1-3) using primary amine initiators. Kinetic studies of polymerization revealed a first-order dependence on the monomer concentration, consistent with a living polymerization. The obtained PEGylated polypeptoids are highly hydrophilic with good water solubility (> 200 mg/mL) and are amorphous with the glass transition temperature (T_g) in -41.1-46.4 ^oC range that increases with increasing molecular weight and decreasing side chain length. The DLS and SANS analysis revealed no appreciable adsorption of lysozyme to PNMeOEtG. PNMeOEtG having different molecular weight exhibited minimal cytotoxicity towards HEp2 cells. These combined results suggest the potential use of PEGylated polypeptoids as protein- resistant materials in the biomedical and biotechnological field.

INTRODUCTION

Non-specific protein adsorption to the surface of biomaterials and medical devices accompanied by slow protein denaturation can induce cascades of biological responses upon contact with human blood, including thrombosis, chronic inflammation and fast immunological recognition.[1-4] These biological responses may hinder the function of biomedical devices or materials (*e.g.*, the efficacy of drug delivery vehicles).[1-4] Enhanced resistance to nonspecific protein adsorption, therefore, is critical to the development of synthetic materials towards various biomedical and biotechnological applications (*e.g.*, tissue engineering, therapeutic delivery and implant devices)

While the mechanisms of non-specific protein adsorption to surfaces are not fully understood,[3] the balance of various non-covalent interactions (*e.g.*, van der Waals, electrostatic and hydrophobic forces) between a protein and a surface is considered to be important.[3] The water layer bound to hydrophilic polymer chains is often considered responsible for inhibiting protein adsorption.[4-5] Based on the reported studies, protein-resistant materials usually share a set of molecular characteristics, the so-called "Whitesides rules": 1) hydrophilicity, 2) the presence of hydrogen bond acceptor groups, 3) the absence of hydrogen bond donor groups, and 4) the absence of net charge. [4, 6-7] The "Whitesides rules" have been widely applied for the rational design of protein-resistant materials. Many types of protein-resistant materials have been developed and characterized for their antifouling behaviors. This includes poly(ethylene glycol) (PEG),[3, 8] oligo/polypeptides,[9-10] polycarbonates,[11] polyoxazolines,[12-14] polyacrylamides[15-17] and zwitterionic polymers[3, 18-19]. Among them, PEG is considered as the gold standard of protein-resistant stealth polymers in polymer-based therapeutic delivery. The drug-PEG conjugates enhance the water solubility of drugs and decrease their interaction with blood components,

leading to increased circulation half-life and decreased toxicity of drugs. However, PEG has notable drawbacks including non-biodegradability, potential immunological recognition and hypersensitivity provocation, as well as accumulation in tissue when the molecular weight of PEG exceeds 40 KDa.[3-4, 8] Zwitterionic polymers (*e.g.*, zwitterionic polycarbonates[18] and polybetaines[3]) which form a very stable hydration shell through strong ion-dipole interaction with water are very promising protein-resistant materials.[3-4] They are minimally soluble in most common organic solvents, rendering the process of conjugating these polymers to hydrophobic drugs more complex relative to that of non-ionic polymers.[11] Polyoxazolines (*e.g.*, poly(2-methyl-2-oxazoline)), while exhibiting similar stealth behavior as PEG, is not backbone degradable. The potential formation of poly (ethylene imine) from enzymatic degradation of the amide bonds on the polyoxazolines side chain can lead to cytotoxicity.[14, 20-21] Polyacrylamides are another category of protein-resistant polymers that is not backbone degradable. In addition, the thermo-responsive characteristic of poly(*N*-isopropylacrylamide) in particular enhances protein adsorption at physiological temperature due to the increased dehydration and hydrophobicity at higher temperature.[15-16, 22] While oliogomeric[23-26] and polymeric peptides[9, 27-28] exhibiting stealth behavior are enzymatically degradable, their water solubility is pH dependent (*e.g.*, in the case of poly-L-lysine and poly-L-aspartate) and the circulation lifetime is reduced when aggregation with oppositely charged biomolecules occurs.[29-30] In addition, proteolysis of peptides reduces their *in vivo* half-lives, limiting their use in long-term biological application (*e.g.*, long-term drug delivery). Polycarbonates have attracted considerable attention in the recent years due to their low toxicity, potential cytocompatibility and biodegradability;[31] however, studies showed that polycarbonates are prone to fast degradation (within several days or weeks) both hydrolytically[32-33] and enzymatically[34] and thus limit their long-term biological use.

Poly (*N*-substituted glycine) (*a.k.a.* polypeptoids), with an *N*-substituted polyglycine backbone, are structural mimics of polypeptides. In contrast to polypeptides, which adopt secondary structures (*e.g.*, helix or sheet) stabilized by hydrogen bonding, polypeptoids lack extensive hydrogen bonding and stereogenic centers on the backbone. These structural characteristics render polypeptoids thermally processable, readily soluble in common organic solvents, and more resistant towards enzymatic and hydrolytic degradation relative to polypeptides.[23-25, 35-36] In addition, early studies showed that polypeptoids exhibit minimal cytotoxicity,[37-40] and are degradable under oxidative conditions that mimics tissue inflammation.[40] The combination of these properties makes polypeptoids attractive for biomedical and biotechnological applications.[35, 41-45] In recent years, oligo polypeptoids ($DP_n \leq 20$) (*e.g.*, polysarcocine,[46] poly(*N*-methoxyethyl glycine),[47-48] poly(*N*-hydroxyethyl glycine)[48]) grafted onto TiO_2 surface through a DOPA-Lys surface anchor have been shown to exhibit excellent antifouling characteristics in inhibiting protein (*e.g.*, human fibrinogen) adsorption and cell (*e.g.*, mammalian cell) attachment. The chain length of polypeptoids obtained by solid-phase synthesis is limited to less than 50 mer.[43] Polysarcosine brushes obtained by surface-initiated ring-opening polymerization (SI-ROP) of sarcosine-derived *N*-carboxyanhyride (Me-NCA) also exhibited antifouling properties.[49] Early studies of antifouling polypeptoids have all been focused on polypeptoids anchored on various surfaces. There is no study on the interaction of soluble polypeptoids with protein in solution.

In this contribution, we report the design and synthesis of a series of structurally well-defined polypeptoids bearing oligomeric ethylene glycol side chains by primary amine-initiated ring-opening polymerization of the corresponding *N*-substituted *N*-carboxyanhydrides (Scheme 2). These PEGylated polypeptoids are highly water soluble, charge neutral and have hydrogen

bond accepting groups both on the backbones and side chains, which fulfill all the criteria of the abovementioned "Whitesides rule" for protein-resistant materials. The CellTiter-Blue cell viability assays revealed these PEGylated polypeptoids are minimally cytotoxic towards HEp2 cells. The small-angle neutron scattering (SANS) and dynamic light scattering (DLS) analysis revealed the absence of obvious adsorption of lysozyme to PNMeOEtG in aqueous solution. These results suggested the potential use of PEGylated polypeptoids as protein-resistant materials for biological applications.

EXPERIMENTAL SECTION

General considerations. All chemicals were purchased from Sigma Aldrich and used as received unless otherwise noted. The primary amine (2-(2-methoxyethoxy)ethanamine (**4**) and 2-(2-(2-methoxyethoxy)ethoxy)ethylamine) (**8**) were synthesized in good yields (61.3-67.2%, Figure S7 and S16) by adapting a reported procedue.[50] All the solvents used in monomer preparation and polymerization were purified by passing through alumina columns under argon. Toluene-d_8 was purified by vacuum transfer after stirring over CaH_2 overnight. ^1H and $^{13}C\{^1H\}$ NMR spectra were obtained using a Bruker AV-400 Nanobay spectrometer (400 MHz for ^1H NMR and 100 MHz for $^{13}C\{^1H\}$ NMR) and a Bruker AV-500 spectrometer (500 MHz for ^1H NMR and 125 MHz for $^{13}C\{^1H\}$ NMR) at 298 K. Chemical shifts (δ) given in parts per million (ppm) were referenced to protio impurities or the ^{13}C isotopes of deuterated solvents ($CDCl_3$ and D_2O). High resolution mass spectroscopy (HRMS) spectra were obtained using 6210 ESI-TOF mass spectrometer (Aglient Technologies). The HEPES buffer (0.1 mol/L) used for sample preparation in SANS study was prepared by dissolving a known amount of pure HEPES (2.38 g) powders in D_2O (80 mL) and sodium hydroxide (NaOH) and hydrochloric acid (HCl) were used to adjust the pH of the buffer.

Size-exclusion chromatography (SEC) analysis. SEC analysis of the polypeptoids were performed using an Agilent 1200 system (Agilent 1200 series degasser, isocratic pump, auto sampler and column heater) equipped with three Phenomenex 5 μm, 300 × 7.8 mm columns, a Wyatt OptilabrEX differential refractive index (DRI) detector with a 690 nm light source, and a Wyatt DAWN EOS multiangle light scattering (MALS) detector (GaAs 30 mW laser at λ = 690 nm). DMF with 0.1M LiBr was used as the eluent at a flow rate of 0.5 mL·min^{-1}. The column and detector temperature was set at 25 ^{o}C. All data analysis was performed using Wyatt Astra V 5.3 software. Polymer molecular weight (M_n) and molecular weight distribution (PDI) were obtained by the Zimm model fit of the MALS-DRI data. The absolute polymer molecular weight (M_n) was determined using the measured refractive index increment d*n*/d*c* values. The refractive index increment (d*n*/d*c*) of the polymer was determined using Wyatt OptilabrEX DRI detector and Astra software d*n*/d*c* template. The polymer was dissolved in DMF with 0.1 mol/L LiBr to prepare six dilute solutions with known concentrations (0.05-3.00 mg/mL) using volumetric flasks. The solutions were injected to the DRI detector and the corresponding d*n*/d*c* values were determined from the linear fit of the respective refractive index versus polymer concentration plot. The d*n*/d*c* values measured for PNMeOEtG$_{106}$, PNMe(OEt)$_2$G$_{102}$ and PNMe(OEt)$_3$G$_{106}$ are 0.0633(4), 0.0686(8) and 0.0563(6) mL/g, respectively.

Matrix-assisted laser desorption ionization-time-of-flight (MALDI-TOF) mass spectrometry analysis. The MALDI-TOF MS experiments were conducted on a Bruker ultrafleXtreme tandem time-of-flight (TOF) mass spectrometer equipped with a smartbeam-II ™ 1000 Hz laser (Bruker Daltonics, Billerica, MA). The instrument was calibrated with Peptide Calibration Standard II (Bruker Daltonics, Billerica, MA). A saturated solution of α-cyano-4-hydroxycinnamic acid (CHCA) in methanol was used as the matrix in all measurements. The

polymer samples (10 mg/mL in THF) were mixed with the saturated matrix solutions at 1:1 volume ratio and vortexed thoroughly. The mixtures (1 μL) were deposited onto a 384-well ground-steel sample plate and were allowed to be fully dried prior to measurement using positive reflector mode. Data analysis was carried out using flexAnalysis software.

Thermogravimetric analysis (TGA). TGA analysis of the polypeptoid solid samples was conducted on a TA TGA 2950 under nitrogen at the heating rate of 10 $^{o}C \cdot min^{-1}$. The decomposition temperature (T_d) of the polypeptoids was determined by the temperature of the maximum weight loss rate.

Differential scanning calorimetry (DSC) analysis. DSC analysis of the polypeptoid solid samples was conducted on a TA DSC 2920 calorimeter under nitrogen. The polymer (~5 mg) was sealed into the hermetic aluminum pan and an empty hermetic aluminum pan was used as the reference. The sample containing pans were first heated from -50 ^{o}C to 200 ^{o}C at 10 ^{o}C/min, cooled to -50 ^{o}C at 10 ^{o}C/min and remained at -50 ^{o}C for 5 min and reheated to 200 ^{o}C at 10 ^{o}C/min. The glass transition temperature (T_g) was determined as the temperature corresponding to the minimum of the derivative of the heat flow trace around the glass transition.

Dynamic light scattering (DLS) analysis. $PNMeOEtG1_{06}$, PEG8000 or lysozyme was dissolved in PBS at 1wt% and filtered through 0.22 μm filters before measurements. All the samples were measured using Malvern Zetasizer Nano-zs (Zen3600). The He-Ne laser operating at $\lambda = 633$ nm was utilized, and scattered light intensity was detected at an external angle of 173 ^{o}C using non-invasive backscatter (NIBS) technology. Data from three measurements with 12 scans for each measurement was recorded. The hydrodynamic diameters and PDI of the samples were obtained from cumulant analysis.[51]

Small-angle neutron scattering (SANS) analysis. The SANS studies were performed at the NIST Center for Neutron Research (NCNR) in Gaithersburg, MD, on the NG7 30 m SANS instrument, using neutrons with wavelength λ = 6 Å and wavelength spread, $\Delta\lambda/\lambda$ = 11%. The temperature was maintained at 20 ± 0.1 °C using a circulating bath. A typical SANS data reduction protocol, which consisted of subtracting scattering contributions from the empty cell (2 mm demountable titanium cells), background scattering, and sorting data collected from two different detector distances was used to yield normalized scattering intensities, I(Q) (cm^{-1}) *a.k.a.* the macroscopic scattering cross-section ($d\Sigma/d\Omega$) as a function of the scattering vector, Q ($Å^{-1}$). Data reduction was conducted employing the NCNR Igor-pro platform. The SANS scattering intensity for our macromolecular solution is modelled as [52]

$$\frac{d\Sigma}{d\Omega} = \phi\Delta\rho^2 VP(Q)S(Q) \quad (1)$$

Here, ϕ is the volume fraction of the molecules, $\Delta\rho$ and V, are their average scattering contrast and volume, respectively. The single molecular form factor, $P(Q)$, averaged particle scattering over the ensemble of sizes and orientations, is related to the particle structure. The effective structure factor, $S(Q)$, provides information about the intermolecular interaction. For dilute solutions of non-interacting molecules, $S(Q) \approx 1$. In the current work we have modelled the form factor and the structure for lysozyme molecule using a hard sphere approximation.[53-54] The form factor for the polymer is modelled using the random Gaussian coil.[55]

Synthesis of ethyl 2-((2-methoxyethyl)amino)acetate (1), ethyl 2-((2-(2-methoxyethoxy)ethyl)amino)acetate (5) and ethyl 2-((2-(2-(2-ethoxyethoxy)ethyl)amino)acetate (9). 2-methoxyethylamine (10 g, 0.13 mol) and triethylamine (18.6 mL, 0.13 mol) was dissolved in ethyl acetate (100 mL). Ethyl bromoacetate

(14.7 mL, 0.13 mol) dissolved in ethyl acetate (50 mL) was added dropwise to the above mixture at room temperature and stirred at room temperature for 4 h. The white precipitation was removed by filtration and the filtrate was condensed to obtain the crude product as pale yellow liquid (21.2 g). The crude product was purified by column chromatography performed on silica gel (230-400 mesh, 60 Å, Sorbent Technologies) using ethyl acetate/methanol (R_f = 0.5 in 5% MeOH) as the eluent to afford the desired product as colorless liquid (17.2 g, 82.3% yield). ^{1}H NMR (δ in $CDCl_3$, 400 MHz, ppm): 1.23-1.26 ppm (t, J = 7.16 Hz, 3H, -$COOCH_2CH_3$); 1.87 ppm (s, 1H, -N*H*-); 2.76-2.79 ppm (t, J = 5.12 Hz, 2H, -$CH_2NHCH_2CH_2$-); 3.33 ppm (s, 3H, -OCH_3); 3.40 ppm (s, 2H, -$NHCH_2COO$-); 3.45-3.48 ppm (t, J = 5.08, 2H, $CH_3OCH_2CH_2$-); 4.14-4.19 ppm (q, J = 7.12 Hz, 2H, -$COOCH_2CH_3$). $^{13}C\{^1H\}$ NMR (δ in $CDCl_3$, 125 MHz, ppm): 14.2 ppm (-$COOCH_2CH_3$); 48.8 ppm (-$CH_2NHCH_2CH_2$-); 51.0 ppm (-OCH_3); 58.7 ppm (-$NHCH_2COO$-); 60.7 ppm ($CH_3OCH_2CH_2$-); 72.1 ppm (-$COOCH_2CH_3$); 172.3 ppm (-CH_2COOH). Ethyl 2-((2-(2-methoxyethoxy)ethyl)amino)acetate (**5**) in 68.5-70.5% yield was synthesized by the same procedure as that for the compound **1**. ^{1}H NMR (δ in $CDCl_3$, 400 MHz, ppm): 4.18-4.24 ppm (q, J = 7.12Hz, 2H, -$COOCH_2CH_3$); 3.56-3.65 ppm (m, 6H, $CH_3OCH_2CH_2OCH_2$-); 3.45 ppm (s, 2H, -$NHCH_2COO$-); 3.41 ppm (s, 3H, CH_3O-); 2.83-2.86 ppm (t, J = 10.6 Hz, 2H, -CH_2NHCH_2-); 1.83 ppm (s, -N*H*-); 1.28-1.31 ppm (t, J = 14.3 Hz, 3H, -CH_2CH_3). $^{13}C\{^1H\}$ NMR (δ in $CDCl_3$, 125 MHz, ppm): 172.3 ppm (-$COOCH_2CH_3$); 70.3-71.9 ppm ($CH_3OCH_2CH_2OCH_2$-); 59.0-60.7 ppm (-CH_2COOCH_2-); 48.8-51.0 ppm ($CH_3OCH_2CH_2OCH_2CH_2NH$-); 14.2 ppm (-$COOCH_2CH_3$). Ethyl 2-((2-(2-(2-ethoxyethoxy)ethyl)amino)acetate (**9**) in 66.9-71.6% yield was synthesized by the same procedure as that for compound **1** and **5**. ^{1}H NMR (δ in $CDCl_3$, 400 MHz, ppm): 4.16-4.21 ppm (q, J = 7.12 Hz, 2H, CH_3CH_2COO-); 3.54-3.66 ppm (m, 10H, -$CH_2OCH_2CH_2OCH_2CH_2OCH_3$);

3.44 ppm (s, 2H, -NHCH_2COO-); 3.38 ppm (s, 3H, -OCH_3); 2.80-2.83 ppm (t, 2H, -CH_2NHCH$_2$COO-); 2.09 ppm (bs, 1H, -N*H*-); 1.26-.1.29 ppm (t, 3H, -COOCH$_2$CH_3). ^{13}C{^{1}H} NMR (δ in $CDCl_3$, 125 MHz, ppm): 172.2 ppm (-*C*OO-); 70.3-71.9 ppm (-*C*H$_2$*C*H$_2$O*C*H$_2$*C*H$_2$OCH$_2$CH$_2$NHCH$_2$COO*C*H$_2$-); 59.0-60.7 ppm (-*C*H$_2$CH$_2$NH*C*H$_2$-); 48.8-50.9 ppm (*C*H$_3$OCH$_2$CH$_2$OCH$_2$CH$_2$OCH$_2$*C*H$_2$-); 14.2 ppm (-COOCH$_2$*C*H$_3$).

Synthesis of ethyl 2-((2-methoxyethyl)amino)acetic acid hydrochloride (2), ethyl 2-((2-(2-methoxyethoxy)ethyl)amino)acetate hydrochloride (6) and ethyl 2-((2-(2-(2-ethoxyethoxy)ethyl)amino)acetate hydrochloride (10). Compound **1** (16.5 g, 0.10 mol) was added into an aqueous HCl (104 mL, 4 mol/L) and heated at 80 ^{o}C for 24 h. The water was removed by rotary evaporation to obtain a colorless oil (12.8 g, ~100% yield), which was used directly in the synthesis of compound **3** without further purification. ^{1}H NMR (δ in D_2O, 400 MHz, ppm): 3.25-3.27 ppm (t, J = 4.00 Hz, 2H, -CH$_2$NHCH_2CH$_2$-); 3.30 ppm (s, 3H, -OCH_3); 3.64-3.66 ppm (t, J = 4.00 Hz, 2H, CH$_3$OCH_2CH$_2$-); 3.91 ppm (s, 2H, -NHCH_2COO-). ^{13}C{^{1}H} NMR (δ in D_2O, 125 MHz, ppm): 46.7 ppm (-CH$_2$NH*C*H$_2$CH$_2$-); 47.2 ppm (-O*C*H$_3$); 58.3 ppm (CH$_3$O*C*H$_2$CH$_2$-); 66.7 ppm (-NH*C*H$_2$COO-); 168.8 ppm (-CH$_2$*C*OOH). Ethyl 2-((2-(2-methoxyethoxy)ethyl)amino)acetate hydrochloride (**6**) in ~100% yield was synthesized by the same procedure as that for **2**. ^{1}H NMR (δ in D_2O, 400 MHz, ppm): 3.91 ppm (s, 2H, -NHCH_2COOH); 3.55-3.74 ppm (m, 6H, CH$_3$OCH_2CH_2OCH_2-); 3.31 ppm (s, 3H, CH_3O-); 3.27-3.29 ppm (t, J=9.96 Hz, -C*H*2CH-). ^{13}C{^{1}H} NMR (δ in D_2O, 125 MHz, ppm): 169.0 ppm (-*C*OOH); 65.3-71.0 ppm (CH$_3$O*C*H$_2$*C*H$_2$OCH$_2$CH$_2$NH*C*H$_2$-); 58.0 ppm (-*C*H$_2$CH$_2$NH-); 46.9-47.3 ppm (*C*H$_3$OCH$_2$CH$_2$OCH$_2$*C*H$_2$-). Ethyl 2-((2-(2-(2-ethoxyethoxy)ethyl)amino)acetate hydrochloride (**10**) in ~100% yield was synthesized by the same procedure as that for compound **2** and **6**. ^{1}H NMR (δ in D_2O, 400 MHz, ppm): 3.28-3.29 ppm (m, 5H,

$CH_3OCH_2CH_2OCH_2CH_2OCH_2CH_2$-); 3.53-3.55 ppm (m, 2H, $CH_3OCH_2CH_2OCH_2CH_2OCH_2CH_2$-); 3.61-3.65 ppm (m, 6H, $CH_3OCH_2CH_2OCH_2CH_2$-); 3.74-3.75 ppm (m, 2H, CH_3OCH_2-); 3.92 ppm (s, 2H, $HOOCCH_2$-). $^{13}C\{^1H\}$ NMR (δ in D_2O, 125 MHz, ppm): 46.9-47.2 ppm ($CH_3OCH_2CH_2OCH_2CH_2OCH_2CH_2$-); 58.0 ppm ($CH_3OCH_2CH_2OCH_2CH_2OCH_2CH_2$-); 65.2 ppm ($CH_3OCH_2CH_2OCH_2CH_2$-); 69.4-69.5 ppm ($CH_3OCH_2CH_2OCH_2CH_2$-); 70.9 ppm ($HOOCCH_2$-); 168.9 ppm ($HOOCCH_2$-).

Synthesis of 2-(*N*, *N*-*tert*-butoxycarbonyl-2-methoxyethyl)amino)acetic acid (3), 2-(*N*, *N*-*tert*-butoxycarbonyl-2-(2-methoxyethoxyethyl)amino)acetic acid (7) and 2-(*N*, *N*-*tert*-butoxycarbonyl-2-(2-(2-(2-ethoxyethoxy)ethyl)amino) acetic acid (11). Compound **2** (16.0 g, 0.09 mol), triethylamine (62.7 mL, 0.45 mol) and di-*tert*-butyl dicarbonate (49 g, 0.23 mol) were mixed in distilled water (200 mL) and stirred at 25 ^oC for 24 h. The reaction mixture was extracted with hexanes (2 x 200 mL) to remove extra di-*tert*-butyl dicarbonate. The aqueous phase was acidified with aqueous HCl (4 mol/L) at 0 ^oC and extracted with ethyl acetate (3 x 100 mL). The organic phase was washed with brine (1 x 200 mL) followed by drying over anhydrous $MgSO_4$. After filtration, the solvent was removed to obtain the desired product as white solid (18.5 g, 88.2%). ^1H NMR (δ in $CDCl_3$, 400 MHz, ppm): 1.45-1.49 ppm (d, 9H, $-C(CH_3)_3$); 3.35-3.38 ppm (d, 3H, $-OCH_3$); 3.47-3.53 (m, 2H, $CH_3OCH_2CH_2$-); 3.59-3.61 ppm (m, 2H, $CH_3OCH_2CH_2$-); 4.01-4.09 (d, 2H, HOOCCH2-). $^{13}C\{^1H\}$ NMR (δ in $CDCl_3$, 125 MHz, ppm): 28.2-28.3 ppm ($-C(CH_3)_3$); 48.5-48.7 ppm ($CH_3OCH_2CH_2$-); 50.3-51.6 ppm ($CH_3OCH_2CH_2$-); 58.7-57.4 ppm ($CH_3OCH_2CH_2$-); 71.5-71.6 ppm ($HOOCCH_2$-); 80.9-81.0 ppm ($-C(CH_3)_3$); 155.0-155.8 ppm ($-COOC(CH_3)_3$); 174.2-174.5 ppm ($-CH_2COOH$). 2-(*N*, *N*-*tert*-butoxycarbonyl-2-(2-methoxyethoxyethyl)amino)acetic acid (**7**) in 80.5-82.9% yield was synthesized by the same procedure as that for compound **3**. ^1H NMR (δ in $CDCl_3$, 400 MHz, ppm): 4.03-4.11 ppm (d, 2H,

HOOCCH_2-); 3.48-3.69 ppm (m, 8H, -CH_2CH_2OCH_2CH_2OCH_3); 3.39 ppm (s, 3H, -OCH_3); 1.45-1.48 ppm (d, 9H, -C(CH_3)$_3$). ^{13}C{^{1}H} NMR (δ in $CDCl_3$, 125 MHz, ppm): 28.2-28.4 ppm (-C(*C*H_3)$_3$); 48.4-50.1 ppm (*C*H_3OCH_2CH_2OCH_2*C*H_2-); 58.7-58.8 ppm ($CH_3OCH_2CH_2OCH_2CH_2$-); 69.9-70.5 ppm ($CH_3OCH_2CH_2$-); 71.9-72.0 ppm (HOOC*C*H_2-); 80.5-80.6 ppm (-*C*(CH_3)$_3$); 155.3-155.7 ppm (-*C*OOC(CH_3)$_3$); 172.6-172.7 ppm (-CH_2*C*OOH). 2-(*N*, *N*-*tert*-butoxycarbonyl-2-(2-(2-(2-ethoxyethoxy)ethyl)amino) acetic acid (**11**) in 80.1-84.3 % yield was synthesized by the same procedure as that for compound **3** and **7**. ^{1}H NMR (δ in $CDCl_3$, 400 MHz, ppm): 4.00-4.08 ppm (d, 2H, HOOCCH_2-); 3.47-3.64 ppm (m, 12H, -CH_2CH_2OCH_2CH_2OCH_2CH_2-); 3.39-3.41 ppm (m, 3H, -OCH_3); 1.44-1.47 ppm (d, 9H, -C(CH_3)$_3$). ^{13}C{^{1}H} NMR (δ in $CDCl_3$, 125 MHz, ppm): 28.2-28.3 ppm (-C(*C*H_3)$_3$); 48.5-51.3 ppm (*C*H_3OCH_2CH_2OCH_2CH_2O*C*H_2*C*H_2-); 58.9-59.0 ppm ($CH_3OCH_2CH_2OCH_2$*C*H_2-); 70.1-70.4 ppm (CH_3OCH_2*C*H_2O*C*H_2CH_2-); 71.6-71.8 ppm (HOOC*C*H_2-); 80.7-80.8 ppm (-*C*(CH_3)$_3$); 155.1-155.8 ppm (-*C*OOC(CH_3)$_3$); 173.9 ppm (-CH_2*C*OOH).

Synthesis of MeOEt-NCA (M_1), Me(OEt)$_2$-NCA (M_2) and Me(OEt)$_3$-NCA (M_3). Compound **3** (10.5 g, 0.045 mol) was dissolved in anhydrous dichloromethane (150 mL) under a nitrogen atmosphere. PCl_3 (3.1 mL, 0.036 mol) was added dropwise to the solution at 0 ^{o}C and the mixture was stirred at 25 ^{o}C for 2 h. The solvent was removed under vacuum to obtain yellowish viscous residue. In the glovebox, the residue was extracted with anhydrous dichoromethane (3 x 20 mL) and filtered. The filtrate was stirred with a small amount of sodium hydride to remove any residual moisture. After filtration, the filtrate was condensed to afford a pale yellow liquid (5.7 g, 80.5%). The crude monomer was washed by Soxhlet extraction with hexanes and further purified by distillation (50 ^{o}C, 20-50 militorr (*i.e.*, 2.7-6.7 Pa)) to afford a colorless liquid (4.5 g, 85.1 %). ^{1}H NMR (δ in $CDCl_3$, 400 MHz, ppm): 3.38 ppm (s, 3H, CH_3O-);

3.60 ppm (s, 2H, $CH_3OCH_2CH_2$-); 4.28 ppm (s, 2H, -$OOCCH_2$-). $^{13}C\{^1H\}$ NMR (δ in $CDCl_3$, 125 MHz, ppm): 43.6 ppm ($CH_3OCH_2CH_2$-); 50.8 ppm ($CH_3OCH_2CH_2$-); 59.0 ppm ($CH_3OCH_2CH_2$-); 70.9 ppm (-$OOCCH_2$-); 152.2 ppm (-CH_2OCOOC-); 163.8 ppm (-CH_2OCOOC-). HRMS (ESI-TOF) *m/z* calcd for $C_6H_{10}NO_4$ $[M+H]^+$ 160.0604; found 160.0598. Me(OEt)$_2$-NCA (**M$_2$**) in 60.9-63.8% yield was synthesized by the same procedure as that for compound **M$_1$**. ^1H NMR (δ in $CDCl_3$, 400 MHz, ppm): 4.34 ppm (s, 2H, -$OOCCH_2$-); 3.51-3.72 ppm (m, 8H, -$CH_2CH_2OCH_2CH_2O$-); 3.38 ppm (-OCH_3). $^{13}C\{^1H\}$ NMR (δ in $CDCl_3$, 125 MHz, ppm): 166.1 ppm (-$COOCO$-); 152.3 ppm (-$COOCO$-); 69.4-71.7 ppm (-$OOCCH_2$-, -$CH_2CH_2OCH_2CH_2O$-); 59.1 ppm (-$CH_2CH_2OCH_2CH_2O$-); 50.9 ppm (-$CH_2CH_2OCH_2CH_2O$-); 43.5 ppm (-OCH_3). Me(OEt)$_3$-NCA (**M$_3$**) in 61.1-64.6% yield was synthesized by the same procedure as that for compound **M$_1$ and M$_2$**. HRMS (ESI-TOF) *m/z* calcd for $C_8H_{14}NO_5$ $[M+H]^+$ 204.0866; found 204.0868. ^1H NMR (δ in $CDCl_3$, 400 MHz, ppm): 4.38 ppm (s, 2H, -$OOCCH_2$-); 3.71-3.73 ppm (m, 2H, CH_3OCH_2-); 3.59-3.66 ppm (m, 8H, $CH_3OCH_2CH_2OCH_2CH_2OCH_2$-); 3.53-3.56 ppm (m, 2H, $CH_3OCH_2CH_2OCH_2CH_2OCH_2CH_2$-); 3.39 ppm ($CH_3O$-). $^{13}C\{^1H\}$ NMR (δ in $CDCl_3$, 125 MHz, ppm): 166.1 ppm (-$COOCO$-); 152.4 ppm (-$COOCO$-); 69.4-70.5 ppm ($CH_3OCH_2CH_2OCH_2$-); 71.9 ppm (-$OOCCH2$-); 59.0 ppm ($CH_3OCH_2CH_2OCH_2CH_2$-); 50.9 ppm ($CH_3OCH_2CH_2OCH_2CH_2OCH_2CH_2$-); 43.5 ppm ($CH_3OCH_2CH_2OCH_2CH_2OCH_2CH_2$-). HRMS (ESI-TOF) *m/z* calcd for $C_{10}H_{17}NO_6$ Na $[M+Na]^+$ 270.0948; found 270.0952.

Representative synthetic procedure for PNMeOEtG. In the glovebox, **M$_1$** (56.9 mg, 0.36 mmol, $[M]_0$ = 1 mol/L) was dissolved in anhydrous THF (201 μL). A volume of $BnNH_2$/THF stock solution (157 μL, 91.2 mM, $[M]_0$: $[BnNH_2]_0$ = 25 : 1) was added to the monomer solution and heated at 50 ^oC for 24 h under nitrogen atmosphere to reach quantitative conversion as verified by FT-IR or NMR spectroscopy. The polymerization was quenched by

adding excess hexanes. The precipitate was collected and washed with hexanes, followed by drying under vacuum to obtain a crispy solid. Freeze drying yielded a white fluffy solid (34.1 mg, 82.3%). ^{1}H NMR (δ in D_2O, 400 MHz, ppm): 7.25-7.33 ppm and 2.77-2.82 ppm (benzyl end group); 4.01-4.53 ppm (m, -COCH_2-); 3.49-3.83 ppm (m, -CH_2CH_2OCH_3); 3.02-3.31(d, -$CH_2CH_2OCH_3$). ^{13}C{^{1}H} NMR (δ in $CDCl_3$, 125 MHz, ppm): 169.0-169.8 ppm (-*C*OCH_2-), 71.0-71.4 ppm (-CO*C*H_2-), 69.9 ppm (-CH_2*C*H_2OCH_3), 58.6-59.1 ppm (-*C*$H_2CH_2OCH_3$), 47.2-50.0 pm (-O*C*H_3). (PNMe$(OEt)_2$G (pale yellow sticky liquid) in 87.8-89.1% yield was synthesized by the same procedure as that for PNMeOEtG. ^{1}H NMR (δ in D_2O, 400 MHz, ppm): 7.22-7.32 ppm and 2.93-2.94 ppm (benzyl end group); 4.09-4.63 ppm (m, 2H, -COCH_2-); 3.51-3.60 ppm (m, 8H, -CH_2CH_2OCH_2CH_2OCH_3); 3.26-3.28(m, -OCH_3). ^{13}C{^{1}H} NMR (δ in $CDCl_3$, 125 MHz, ppm): 169.3-169.8 ppm (-*C*OCH_2-), 71.8 ppm (-CO*C*H_2-), 68.3-71.8 ppm (-*C*H_2O*C*H_2*C*H_2OCH_3), 58.9 ppm (-*C*$H_2CH_2OCH_2CH_2OCH_3$), 48.0-49.9 ppm (-O*C*H_3). (PNMe$(OEt)_3$G (pale yellow sticky liquid) in 86.9-89.5% yield was synthesized by the same procedure as that for PNMeOEtG and PNMe$(OEt)_2$G. ^{1}H NMR (δ in D_2O, 400 MHz, ppm): 7.24-7.32 ppm(benzyl end group); 4.10-4.55 ppm (m, 2H, -COCH_2-); 3.53-3.59 ppm (m, 12H, -CH_2CH_2OCH_2CH_2OCH_2CH_2OCH_3); 3.29 (m, -OCH_3). ^{13}C{^{1}H} NMR (δ in $CDCl_3$, 125 MHz, ppm): 169.2-169.8 ppm (-*C*OCH_2-), 71.9 ppm (-CO*C*H_2-), 68.4-70.5 ppm (-*C*H_2O*C*H_2*C*H_2O*C*H_2*C*H_2OCH_3), 59.0 ppm (-*C*$H_2CH_2OCH_2CH_2OCH_2CH_2OCH_3$), 48.0-49.9 ppm (-O*C*$H_3$).

Kinetic studies of $BnNH_2$-initiated ring-opening polymerization of Me $(OEt)_n$-NCA (n = 1-3) (M_1, M_2 and M_3). A predetermined amount of $BnNH_2$ stock solutions in toluene-d_8 were added to a toluene-d_8 solution of Me$(OEt)_n$-NCA (n = 1-3) ($[M]_0$ = 0.2 mol/L, $[M]_0$:$[BnNH_2]_0$ = 25:1) at room temperature followed by transferring into a resealable J-Young

NMR tube. ^{1}H NMR spectra were collected every 3 min 44 s at 50 ^{o}C to determine the conversion of monomers for more than four half-lives. Kinetic experiments were repeated twice for each monomer.

Studies of M_n versus polymerization conversion. The polymerization of Me(OEt)$_n$-NCA (n = 1-3) (**M$_1$**, **M$_2$** and **M$_3$**) was conducted in THF at 50 ^{o}C ([M]$_0$:[I]$_0$ = 50:1, [M]$_0$ = 1 mol/L) and aliquots were taken at different time intervals and analyzed by ^{1}H NMR spectroscopy to determine the conversion. The aliquots taken at different time intervals were further analyzed with MALDI-TOF mass spectrometry to obtain the polymer molecular weight (M_n) and molecular weight distribution (PDI). The obtained M_ns were plotted against the corresponding polymerization conversion.

Cytotoxicity study. The cytotoxicity study was conducted by adapting a reported procedure.[56] The HEp2 cells were plated at 8600 cells per well in a Costar 96-well plate (BD biosciences) and allowed to grow for 48 h. The polypeptoids were dissolved in Eagle's Minimum Essential Medium (EMEM) and diluted to final working concentrations (0, 0.0625, 0.125, 0.25, 0.5, and 1.0 mg/mL). The cells were exposed to the working solutions of the polypeptoids in varying concentration and incubated for 24 h (37 ^{o}C, 95% humidity, 5% CO_2). The working solutions were removed, and the cells were washed with 1x PBS. The medium containing 20 % CellTiter Blue (Promega) was added and incubated for 4 h. The viability of cells is measured by reading the fluorescence of the medium at an excitation wavelength of 570 nm and an emission wavelength of 595 nm using a BMG FLUOstar Optima micro-plate reader. In this assay, the indicator dye resazurin is reduced to fluorescent resorufin in viable cells, while non-viable cells are not able to reduce resazurin nor to generate a fluorescent signal. The fluorescence signal of

viable (untreated) cells was normalized to 100%. The mean values are obtained from triplicate measurements.

RESULTS AND DISCUSSION

Synthesis and characterization of Me(OEt)$_n$-NCA and PNMe(OEt)$_n$G (n = 1,2,3). *N*-carboxyanhyride monomers bearing oligomeric ethylene glycol side chains, MeOEt-NCA (**M$_1$**), Me(OEt)$_2$-NCA (**M$_2$**) and Me(OEt)$_3$-NCA (**M$_3$**). Me(OEt)$_n$-NCA (n = 1-3), were synthesized in moderate overall yields (31.3-46.6%) in four steps by adapting a reported procedure[57-58] as outlined in Scheme 1. The monomer precursors (**3, 7** and **11**) exhibit as two sets of rotamers at 25 ^{o}C in $CDCl_3$ due to restricted rotation of the amide bond, as supported by the merging and broadening of the two sets of ^{1}H NMR signals at elevated temperature (50 ^{o}C) (Figure S5, S12 and S21). The chemical structures of the desired monomers (**M$_1$**, **M$_2$** and **M$_3$**) were confirmed by ^{1}H and ^{13}C{^{1}H} NMR spectroscopy analysis (Figure 1, S14-S15 and S23-S24). The polypeptoids bearing oligomeric ethylene glycol side chains (PNMe(OEt)$_n$G, n = 1-3) were synthesized by ring-opening polymerizations of their corresponding monomers (**M$_1$**, **M$_2$** and **M$_3$**) using benzyl amine initiators (Scheme 2). Polymerization reactions were conducted at different initial monomer to initiator ratios ([M]$_0$:[I]$_0$) in anhydrous THF at 50 ^{o}C for 24-48 h to reach quantitative conversion. The polymers were purified by precipitation in hexanes and collected by filtration followed by drying under vacuum to yield ether crispy white solids (PNMeOEtG) or viscous liquids (PNMe(OEt)$_n$G, n = 2-3) in good yields (82.3-87.8%). The number-averaged molecular weight (M_n) and degree of polymerization (DP$_n$) of the polymer were determined by both end-group analysis using ^{1}H NMR spectroscopy and SEC-MALS-DRI analysis using the measured d*n*/d*c* values of the polymers. For example, the DP$_n$ and M_n of PNMeOEtG were determined by the integrations at 4.01-4.52 ppm due to the methylene group in the backbone

relative to the integration of signals at 7.3 ppm due to the benzyl end-group (Figure 2). The PNMe(OEt)$_n$G (n = 1-3) were also characterized by $^{13}C\{^1H\}$ NMR spectroscopy (Figure 2, S26-28). The molecular weight of the polymers (M_n) was shown to increase as the initial monomer to initiator ratio ($[M]_0$:$[I]_0$) was systematically increased (Table 1). The polymer molecular weights (M_n) agreed well with the theoretically predicted values at low molecular weight range ($[M]_0$:$[I]_0$ < 200:1). However, at high $[M]_0$:$[I]_0$ ratios (200:1 and 400:1), the molecular weight of the polymers (M_n) determined from SEC analysis deviated from the theoretical values presumably due to the presence of nucleophilic impurities which can initiate the polymerization of these monomers. The polymer molecular weight distributions were narrow with low polydispersity indices (PDI) in the 1.03-1.10 range (Table 1, Figure 3, S31 and S33) as determined by SEC-MALS-DRI analysis in 0.1 mol/L LiBr/DMF at room temperature (20 °C). Similar M_n and PDI control was also observed for the polymerization of MeOEt-NCA conducted in toluene under identical conditions (Table S1). The structure of low molecular weight PNMe(OEt)$_n$G (n = 1-3) was further confirmed by MALDI-TOF MS analysis. The MS spectra revealed a symmetric monomodal set of mass ions where *m/z* equals to integral numbers of the desired repeating unit mass (115.1, 159.1 and 203.1 g/mol) for (PNMe(OEt)$_n$G, n = 1-3) plus 22.99 or 38.96 for sodium or potassium ion. This is consistent with the targeted polypeptoid structures bearing one benzyl amide and one secondary amine chain end (Scheme 2), in support of controlled polymerization initiated by benzyl amine initiator. (Figure 4, S30 and S32). In addition, a minor set of mass ions that are consistent with polypeptoid structures having acyl chloride and amine end-group structures are visible in the expanded spectrum of PNMe(OEt)$_2$G (Figure S30C), indicating Cl^- ions are potential impurities that can initiate the polymerization of the NCAs.

Scheme1. Synthetic procedures of $Me(OEt)_n$-NCA (n = 1-3).

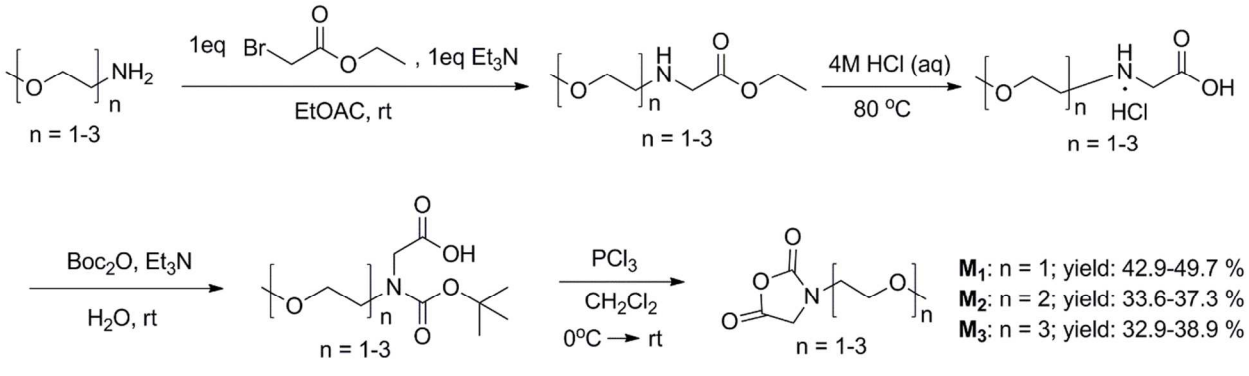

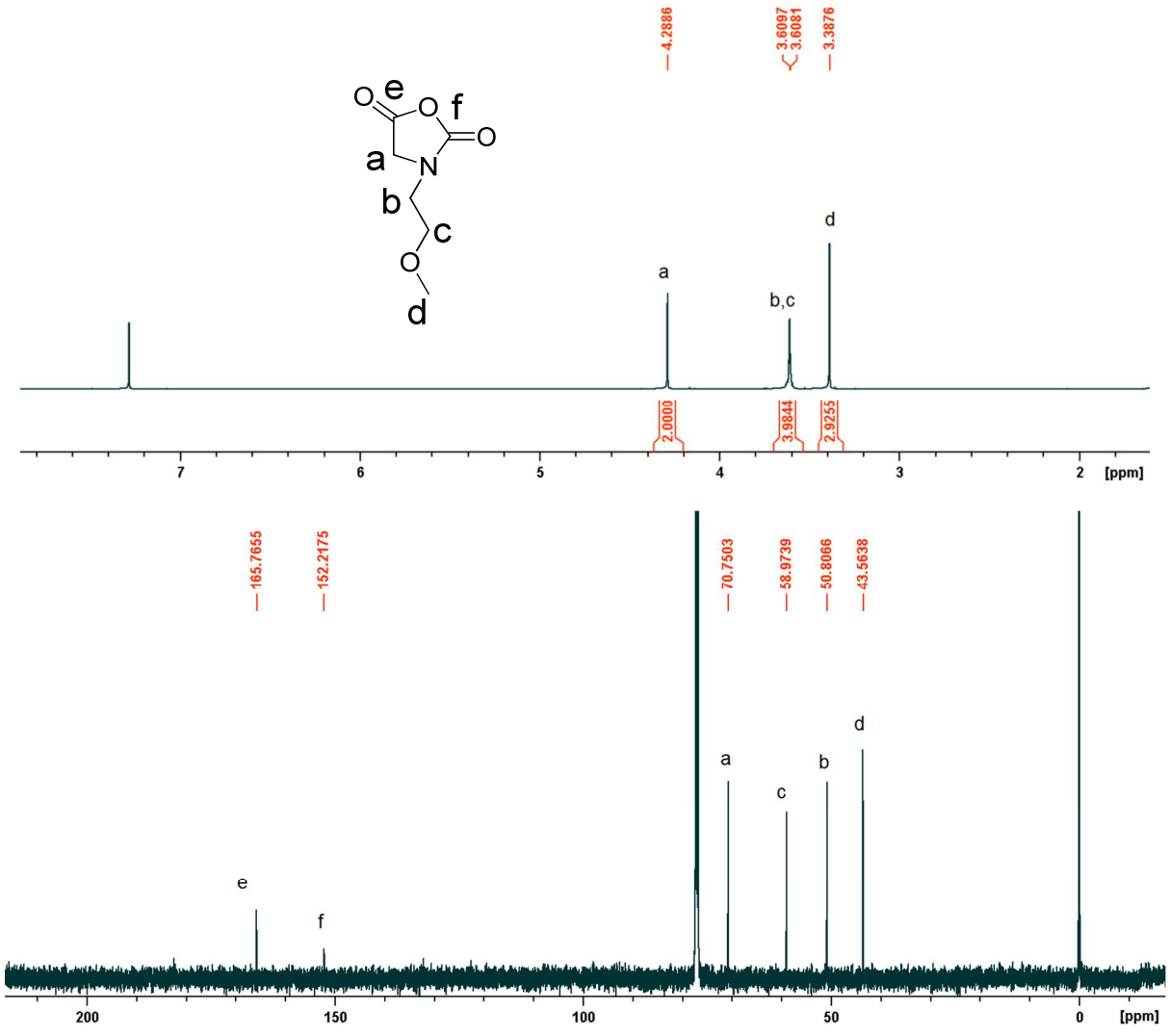

Figure 1. ^1H and $^{13}C\{^1H\}$) NMR spectra of MeOEt-NCA ($\mathbf{M_1}$) in $CDCl_3$.

Scheme 2. Benzyl amine-initiated ROP of $Me(OEt)_n$-NCA (n = 1-3).

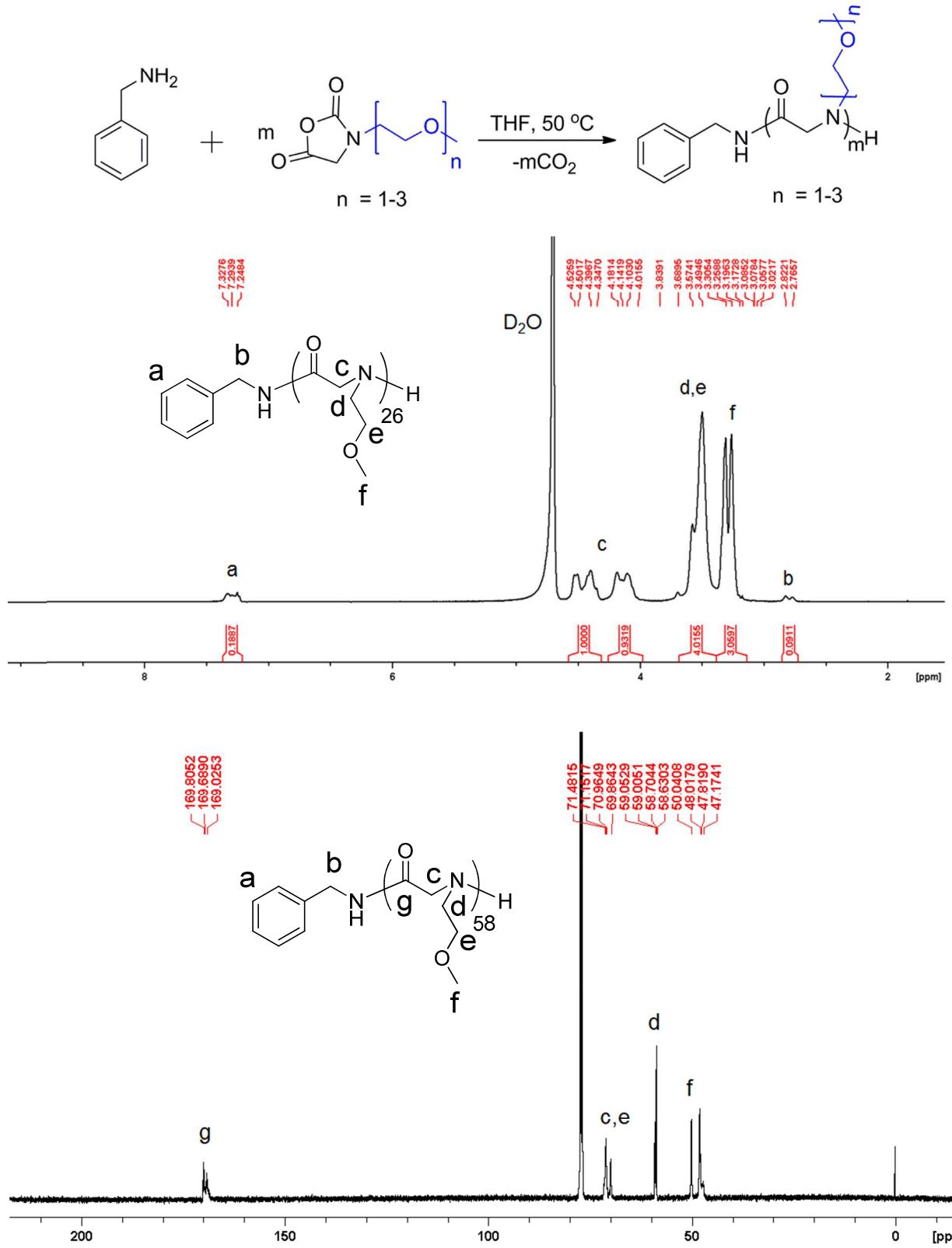

Figure 2. ^{1}H NMR spectrum of $PNMeOEtG_{26}$ in D_2O and $^{13}C\{^{1}H\}$) NMR spectrum of $PNMeOEtG_{58}$ in $CDCl_3$.

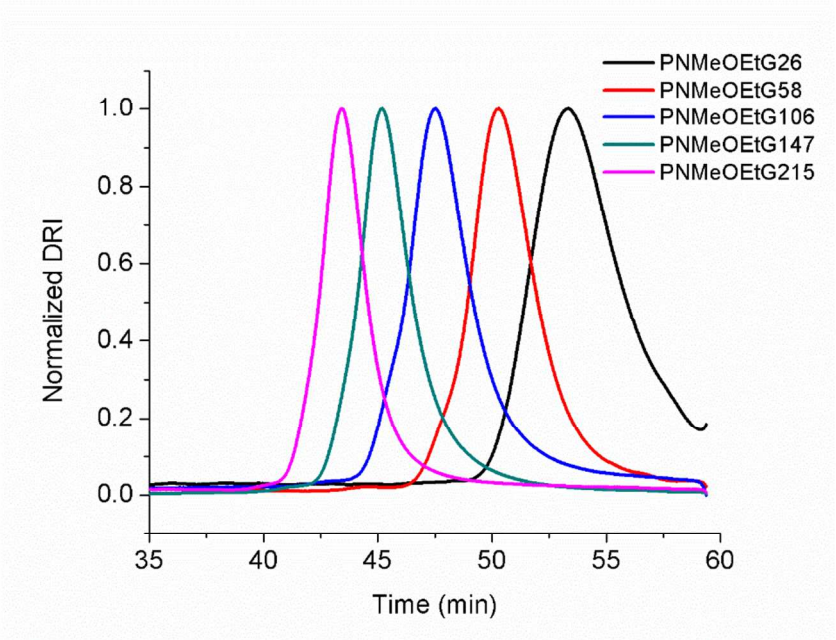

Figure 3. SEC-DRI chromatograms of PNMeOEtG polymers prepared from benzyl amine-initiated polymerization of MeOEt-NCA (**M_1**) ($[M_1]_0$:$[BnNH_2]_0$ = 25:1 (—), 50:1 (—), 100:1 (—), 200:1 (—), 400:1 (—), Table 1). The DP_ns listed in the figure were determined from the SEC-MALS-DRI analysis of the polymers using the d*n*/d*c*= 0.0633(4) mL/g in 0.1 mol/L LiBr/DMF at 20 °C.

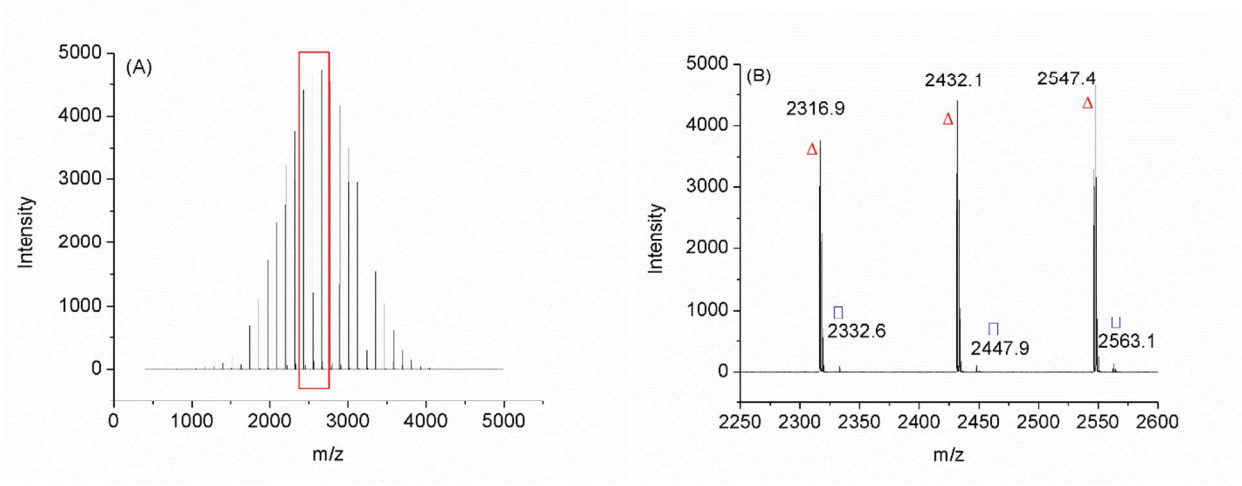

Figure 4. Representative full (A) and expanded MALDI-TOF MS (B) spectra of PNMeOEtG (M_n = 2.7 kg/mol, PDI = 1.03, matrix: CHCA).

Table 1. $BnNH_2$-initiated ROP of MeOEt-NCA (**M_1**), $Me(OEt)_2$-NCA(**M_2**) and $Me(OEt)_2$-NCA(**M_3**).[a]

	Entry	$[M]_0/[I]_0$	M_n (theor.) (kg/mol)[b]	M_n (kg/mol)		PDI[c]	Reaction time (h)	Conv.(%)
				SEC[c]	NMR[d]			100
PNMeOEtG	1	25:1	2.98	3.26	3.09	1.10	24	100
	2	50:1	5.86	6.26	6.32	1.08	24	100
	3	100:1	11.6	11.1	12.4	1.05	24	100
	4	200:1	23.1	17.0	24.6	1.04	48	100
	5	400:1	46.1	24.8	-[e]	1.04	48	100
$PNMe(OEt)_2G$	1	25:1	4.08	4.03	4.24	1.06	24	100
	2	50:1	8.06	8.57	8.69	1.09	24	100
	3	100:1	16.0	13.5	16.3	1.03	48	100
	4	200:1	31.9	18.9	33.9	1.04	48	100
	5	400:1	63.7	26.8	-[e]	1.05	48	100
$PNMe(OEt)_3G$	1	25:1	5.18	5.29	5.18	1.07	24	100
	2	50:1	10.3	9.34	11.7	1.05	24	100
	3	100:1	20.4	16.9	21.6	1.07	48	100
	4	200:1	40.7	24.2	41.3	1.06	48	100
	5	400:1	81.3	30.0	-[e]	1.08	48	100

[a] All the polymerizations were conducted in THF at 50 °C with $[M]_0$ = 1.0 mol/L. SEC analysis was conducted by directly injecting the polymerization solutions into SEC column after reaching quantitative conversion. [b] Determined based on conversion and $[M]_0/[I]_0$ ratio. [c] Determined from a tandem SEC-MALS-DRI system using the d*n*/d*c* 0.0633(4) mL/g for PNMeOEtG, 0.0686(8) mL/g for $PNMe(OEt)_2G$ and 0.0563(6) mL/g for $PNMe(OEt)_3G$ in 0.1 mol/L LiBr/DMF at room temperature. [d] Determined by the end-group analysis using ^1H NMR spectroscopy. [e] The benzyl amine end-group content is too low to be accurately integrated and therefore the M_n cannot be reliably determined from the ^1H NMR end-group analysis.

Polymerization kinetics were investigated at a constant initial monomer to initiator ratio ($[M]_0$:$[BnNH_2]_0$ = 25:1, $[M]_0$ = 0.2 mol/L) in toluene-d_8 at 50 °C. The polymerizations of the three monomers all exhibited a first-order dependence on the monomer concentration (*i.e.*,

d[M]/dt = k_{obs}[M]), consistent with a living polymerization (Figure 5). As the number of ethylene glycol unit on the monomer side chain increased from one (MeOEt-NCA, $\mathbf{M_1}$) to three (Me$(OEt)_3$-NCA, $\mathbf{M_3}$), the observed rate constant (k_{obs}) of the polymerization decreased from 0.01285(±6) to 0.00291(±7) min^{-1}. It was attributed to the enhanced steric hindrance and electron-withdrawing effect associated with the increased number of ethylene glycol moiety on the side chain (from $\mathbf{M_1}$ to $\mathbf{M_2}$ and $\mathbf{M_3}$), resulting in reduced nucleophilicity of the secondary amino chain end and thus decreasing propagation rate. In addition, the plots of M_n of the corresponding polypeptoids all exhibited a linear dependence on polymerization conversion (Figure 5B and S33), indicating the presence of a constant concentration of propagation species in accord with a living polymerization. The molecular weight distribution (PDI = 1.01-1.18) determined by MALDI-TOF MS analysis remained relatively narrow throughout the course of polymerization.

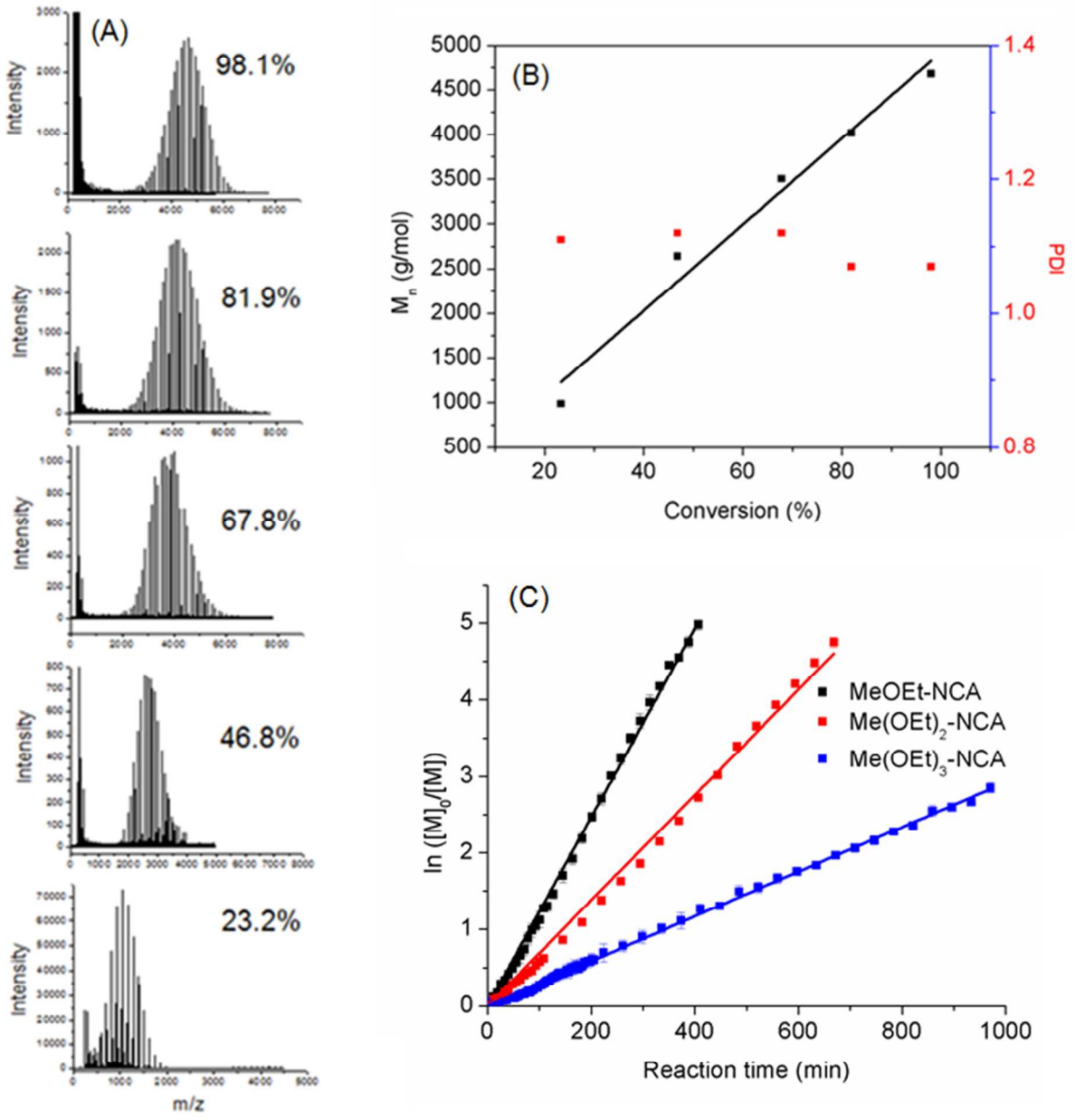

Figure 5. (A) MALDI-TOF MS spectra of PNMeOEtG (PDI = 1.07-1.11) at different polymerization conversion. (B) Plots of M_n and PDI verses conversion for $BnNH_2$-initiated polymerization of MeOEt-NCA in THF ($[M]_0$:$[I]_0$ = 50:1, $[M]_0$ = 1 mol/L). (C) Plots of ln ($[M]/[M]_0$) versus the reaction time for the $BnNH_2$-initiated polymerization of $Me(OEt)_n$-NCA (n = 1-3) ($[M]_0$:$[BnNH_2]$ = 25:1, $[M]_0$ = 0.2 mol/L, in toluene-d_8 at 50 ^oC). The error bars in (C) are the standard deviation of three measurements.

DSC and TGA analysis of (PNMe(OEt)$_n$G, n = 1-3). The PEGylated polypeptoids were characterized by TGA and DSC. The TGA thermograms of PNMe(OEt)$_n$G100 (n = 1-3) (Figure 6 (A), S34 and S35) revealed a three-stage decomposition profiles with a slow and gradual mass loss at low temperatures (25-100 ^oC) which was attributed to the loss of small amount of water in the samples due to the highly hygroscopic nature of these polymers, followed by a drastic mass loss occurring at 250-400 ^oC for all three PEGylated polypeptoids and then a gradual decrease of mass loss from 400-500 ^oC. These data indicated the decomposition temperatures (T_d) of the three polymers are all higher than 250 ^oC. As a result, the subsequent DSC analysis was conducted in the temperature window between -50 ^oC and 200 ^oC. The DSC thermograms of the three polymers from the second heating cycle are shown in Figure 6, S36 and S37. The absence of melting and crystallization exothermic peaks indicates that all three PEGylated polypeptoids (M_n = 3.26-16.9 kg/mol) are amorphous, in agreement with the previously reported oligomeric PEGylated peptoids.[50] The T_g values of the PEGylated polypeptoids (Table 2) decreased with increasing the length of oligomeric ethylene glycol side chains PNMeOEtG (T_g = 24.5 – 46.4 ^oC) > PNMe(OEt)$_2$G (T_g = -5.8 – -15.8 ^oC) > PNMe(OEt)$_3$G (T_g = -34.9 – -41.1 ^oC), consistent with the previously reported observations for the oligomeric analogs.[50] The decrease of T_g with increasing side chain length has also been observed for comb-like polymers having *n*-alkyl side chains of varying length and semi-flexible or rigid main chains.[59] Dynamic asymmetry between backbone and side chain have been attributed to the T_g dependence on the side chain length.[60-63] The T_g values observed for all the PEGylated polypeptoids were significantly lower than that of the amorphous poly(*N*-methyl glycine) (*a.k.a.* polysarcosine) (T_g = 127-143 ^oC) and poly(*N*-ethyl glycine) (T_g = 93-114 ^oC) having comparable molecular weight.[64] The T_g values of the polymer was shown to increase with the increase of the polymer molecular weight, which is

attributed to the reduction of free volume due to the diminished chain-end content at increasing molecular weight.[65] T_g of $PNMeOEtG_{20}$ polymer (T_g = 24.5 °C, DP_n = 20, PDI = 1.09) is about 14 °C lower than the corresponding 20 mer (T_g = 38.6 °C, PDI < 1.0003) obtained by the solid-phase "submonomer" method.[50] The discrepancy is presumably resulted from the difference in end-group structures and polydispersity of the samples. As the chains are relative short, end-group structural difference will contribute significantly to a difference in free volume and thus T_g. The polymeric sample contains a mixture of chains that are shorter or longer than 20 mer in varying amounts, which will have different T_gs due to free volume difference.

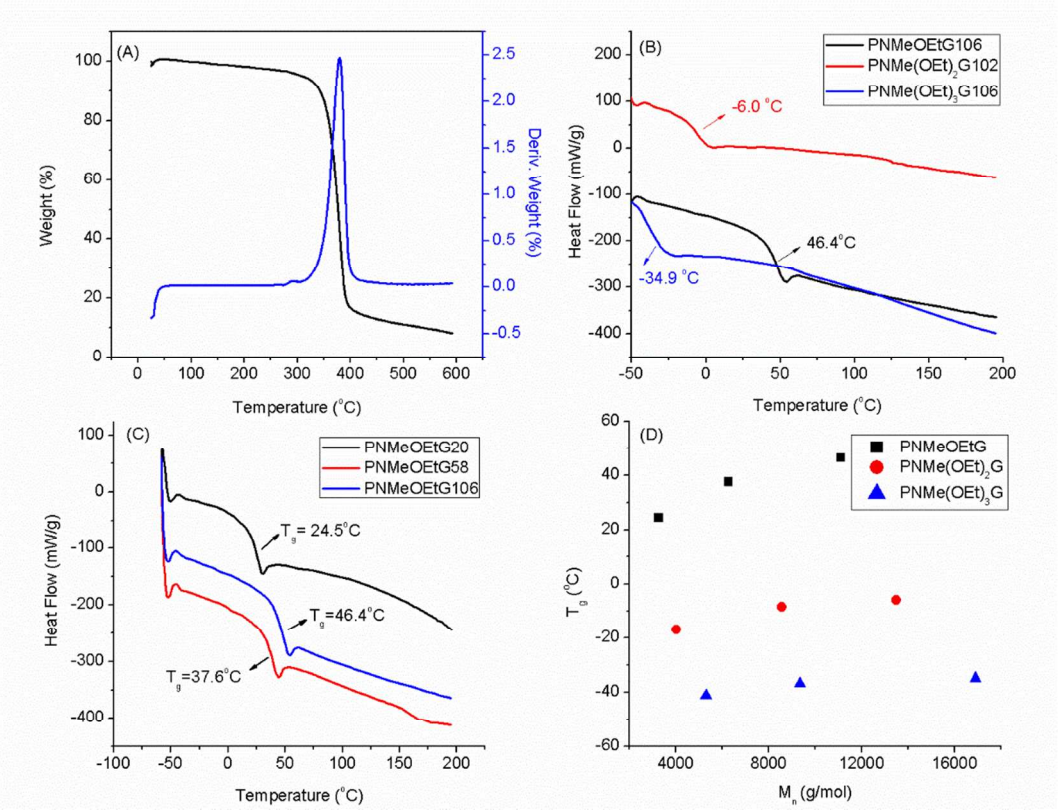

Figure 6. (A) Thermogravimetric analysis (TGA) of $PNMeOEtG_{106}$. (B) DSC thermograms of $PNMe(OEt)_nG$ (n = 1-3). (C) DSC thermograms of PNMeOEtG at different molecular weight

during the second heating cycle. (D) Plot of T_g verses M_n of PNMe(OEt)$_n$G (n=1-3). The DP$_n$s listed in the figures were determined from the end-group analysis by ^{1}H NMR spectroscopy.

Table 2. T_g of PNMe(OEt)$_n$G (n=1-3) at different molecular weight.

Sample	M_n (kg/mol)	T_g (^{o}C)	T_d (^{o}C)
PNMeOEtG	2.41	24.5	378
	6.26	37.6	373
	11.1	46.4	375
PNMe(OEt)$_2$G	4.03	-15.8	345
	8.57	-8.6	345
	13.5	-5.8	360
PNMe(OEt)$_3$G	5.29	-41.1	374
	9.34	-36.9	382
	16.9	-34.9	377

Characterization of protein adsorption and interaction with PNMeOEtG by DLS analysis. As the PEGylated polypeptoids are highly water soluble, charge neutral and have hydrogen bond accepting groups both on the backbones and side chains, which fulfill all the criteria of the abovementioned "Whitesides rule" for protein-resistant materials, we hypothesized that the polymers may exhibit antifouling behaviors. PNMeOEtG was selected as the model polymer to study the protein resistant characteristics of the PEGylated polypeptoids. DLS was used to monitor the size change of PNMeOEtG, lysozyme and their mixture in PBS. Lysozyme was selected here as the model protein due to their comparable size with PNMeOEtG. An increase of hydrodynamic size would be expected for the mixture of lysozyme and PNMeOEtG in PBS if appreciable amount of lysozyme was absorbed to the polymer chains. The PNMeOEtG and lysozyme were found to be stable at their respective 1 wt% solution in PBS during a period of 24 h, evidenced by no appreciable change of the hydrodynamic size distribution and the derived count rates (Figure S38 and S39). The mixture of lysozyme (1 wt%) and PNMeOEtG (1 wt%) in PBS also revealed no obvious hydrodynamic size increase during a period of 24 h.

Furthermore, the hydrodynamic sizes (D_h =5.56 ± 0.16 nm), derived count rates and correlograms of the mixture lie in between that of 1 wt% PNMeOEtG (6.39 ± 0.09 nm) and 1wt% lysozyme (4.69 ± 0.25 nm) individually in PBS, indicating there is no apparent adsorption of lysozyme onto the polymers (Figure 8). For comparison purposes, PEG (M_n = 8000 g/mol), a well-known antifouling material, was similarly investigated for protein adsorption by DLS analysis. The hydrodynamic sizes (D_h = 5.48 ± 0.10 nm (n=3)), derived count rates and correlograms of the PEG8000 (1 wt%) and lysozyme (1wt%) mixture also lie in between that of 1 wt% PEG8000 (5.84 ± 0.40 nm (n=3)) and 1 wt% lysozyme (4.69 ± 0.25 nm (n=3)) in PBS (Figure S40). These results support that the PEGylated polypeptoids do not adsorb appreciably to lysozyme.

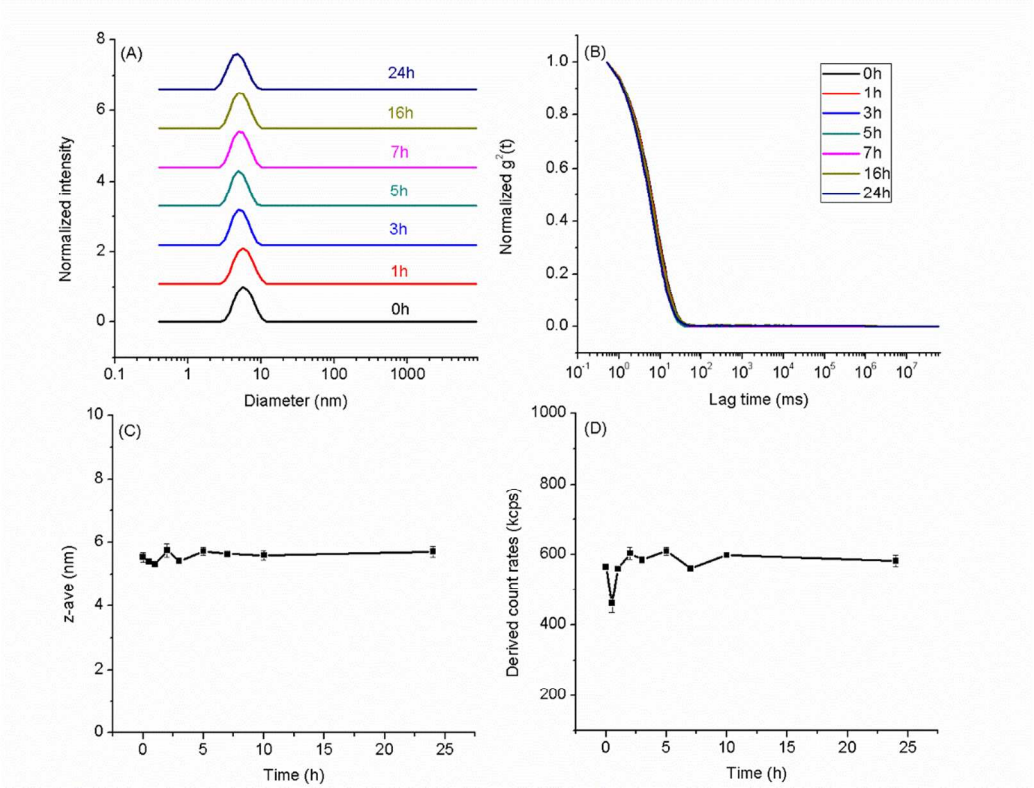

Figure 7. DLS analysis of mixture of 1 wt% lysozyme and $PNMeOEtG_{106}$ in PBS: hydrodynamic size distributions (A, C), correlograms (B) and derived count rates (D) up to 24 h. The error bars in (C) and (D) are the standard deviations of three measurements.

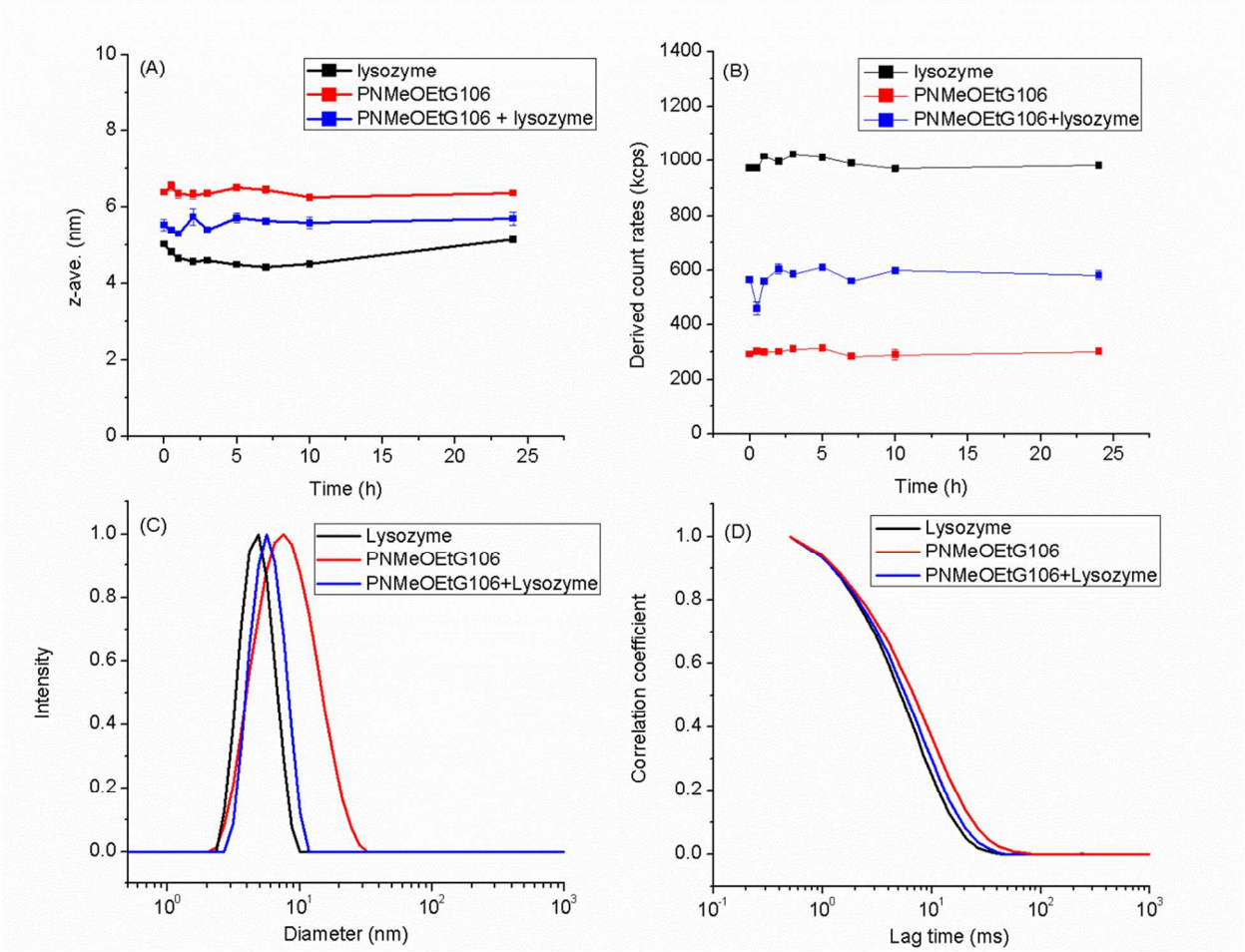

Figure 8. DLS analysis of mixture of 1 wt% $PNMeOEtG_{106}$, 1 wt% lysozyme, 1 wt% lysozyme and 1 wt% $PNMeOEtG_{106}$ in PBS: hydrodynamic size distributions (A) and derived count rates (B) up to 24 h; hydrodynamic size distributions (C) and correlograms (D) at 5h. The error bars in (A) and (B) are the standard deviations of three measurements.

Characterization of protein adsorption and interaction with PNMeOEtG by SANS analysis. The interaction between PNMeOEtG and lysozyme was further investigated by SANS

studies in HEPES buffer. The data presented in Figure 9 is after background subtraction of the HEPES buffer.

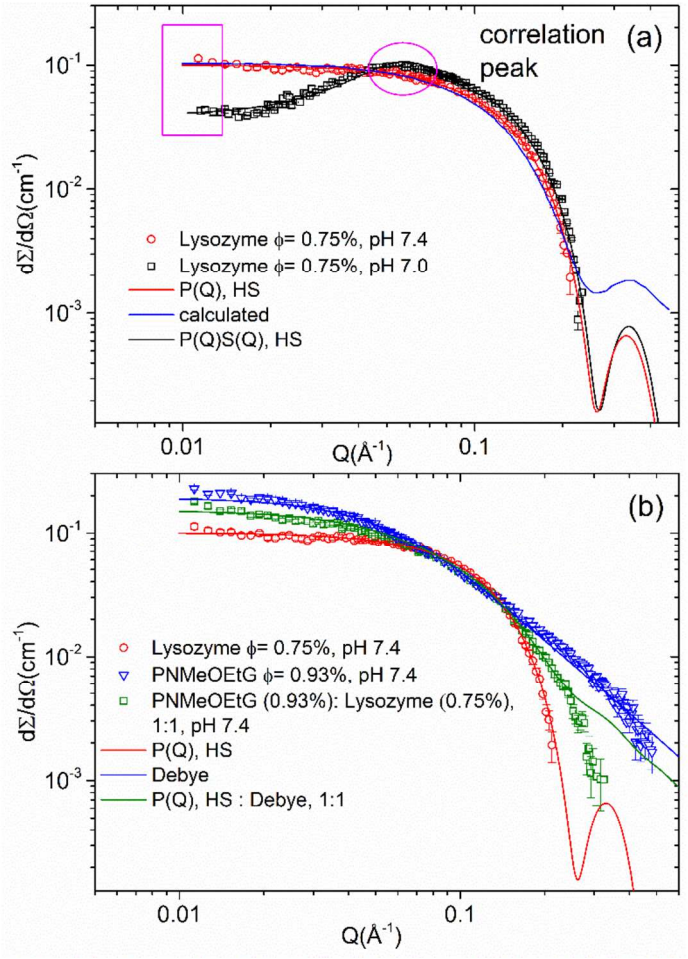

Figure 9. SANS diffraction pattern: (a) lysozyme in HEPES buffer for different pH values (pH 7. 4: ○; pH 7.0: □). The solid lines are the fits using equation (1): the red solid line (—) is the lysozyme modelled using a hard sphere (HS) form factor (P(Q), HS) for structure factor S(Q) = 1 at pH 7.4; the blue solid line (—) is the modelled form factor calculated from the atomic coordinates of the lysozyme; the black solid line (—) is the lysozyme modelled using a product of HS form factor and a repulsive HS structure factor (percuss Yevick approximation) at pH 7.0. (b) Comparison of the scattering pattern among lysozyme (○), polymer (PNMeOEtG) (▽) and

1:1 lysozyme – polymer mixture (□) all at pH 7.4. The solid lines are the fits using equation (1) (S(Q) = 1) for HS P(Q) in red (—), for Gaussian polymer coil (Debye) in blue (—) and for 1:1 mixture of polymer and lysozyme in green (—).

Figure 9(a) represents the SANS diffraction data for the lysozyme at pH 7.0 and 7.4. The rectangular highlighted box at low Q shows an increase in scattering, suggesting formation of aggregates or clusters (attractive interaction) for pH 7.4 and less pronounce for pH 7.0. In addition, surprisingly unique to pH 7.0, at $Q = 0.057$ Å^{-1} there is an evolution of a correlation peak that indicates repulsive interaction. Following equation (1) the data at pH 7.4 was modelled (solid red line) using a hard sphere (HS) form factor (P(Q), HS) for $S(Q) = 1$.[66] The data at pH 7.0 was modelled (solid black line) using a product of HS form factor and a repulsive HS structure factor (Percuss Yevick approximation).[53-54] The modelled form factor is in good agreement with that calculated from the atomic coordinates of the lysozyme (Figure 9a, solid blue line).[67-69] The HS form factor for the lysozyme yields a radius of R_L = 1.71 ± 0.01 nm which is in agreement with the literature report. We did not find difference in size while modelling with an ellipsoidal form factor as was used by Shukla *et al.*[69] The lysozyme contrast with respect to D_2O is calculated to be, $\Delta\rho \sim 2.6 \times 10^{10}$ cm^{-2}, for the density of 1.32 g/cm^3.[70] It should be noted that from the model fitting of the data at pH 7.0 yield a HS S(Q) interaction radius, R_C = 4.85 ± 0.02 nm, which is ~ 2.8 times larger than R_L. This suggests the formation of clusters as a result of lowering of the pH value (from 7.4 to 7.0) is responsible for the structure factor peak in Figure 9 (a). Formation of clusters was also reported first by Stradner *et al.*[67] and later by Shukla *et al.*,[69] for lysozyme solutions. Stradner *et al.*[67] also reported that the S(Q) peak position was found to be independent of the lysozyme concentration. The driving force for cluster formation in proteins is the balance between the short-range attraction and long range electrostatic repulsion. The net

charge of the protein as known from the titration experiment is approximately +8.5*e* and +8.0e for pH 7.0 and 7.4, respectively.[71] Therefore decrease in pH causes an increase in the repulsive interaction (protein surface charge) between the clusters that causes a sharp decrease in the *overall* forward scattering intensity, $\frac{d\Sigma}{d\Omega}(Q \to 0)$, which is manifested as a structure factor (correlation) peak seen in the data at pH 7.0. Following Stradner *et al*.[67] we can argue that the correlation peak reveals the distance between the clusters (cluster-cluster interaction length ~ $2R_C$) but not the individual lysozyme molecules.

In Figure 9 (b) a comparison of the SANS pattern for a mixture of lysozyme and PNMeOEtG polymer is presented. For the pure polymer the form factor was modelled using a Debye function that describes a random Gaussian coil[55] and the structure factor $S(Q)$ equals to 1 in equation 1. It yields a radius of gyration, R_g = 2.62±0.02 nm. The corresponding open square data, represents the 1:1 mixture of the polymer and the lysozyme in a pH 7.4 buffer solution. The data can be modelled by calculating the 1:1 ratio of the scattering pattern obtained from the Debye function for the polymer and the HS form factor for the lysozyme. This clearly supports the absence of any interaction between the polymer and the lysozyme, resulting in the scattering curve of the binary mixture a simple summation of the individual scattering component. It should be noted that these are in contrast to the previous study on the solution mixture of haemoglobin and PEO, where notable interaction between the protein and polymer was observed.[72]

Cytotoxicity study. The cytotoxicity of the PNMeOEtG polypeptoids was assessed using HEp2 cells by the MTT assay. PEG (8000 g/mol), a gold standard for antifouling material, is used as a positive control. The PNMeOEtG having different molecular weight (3.26-11.1 kg/mol) showed minimal cytotoxicity towards HEp2 cells with more than 90% cell viability in the 0.0625 -1.0 mg/mL polymer concentration range (Figure 10).

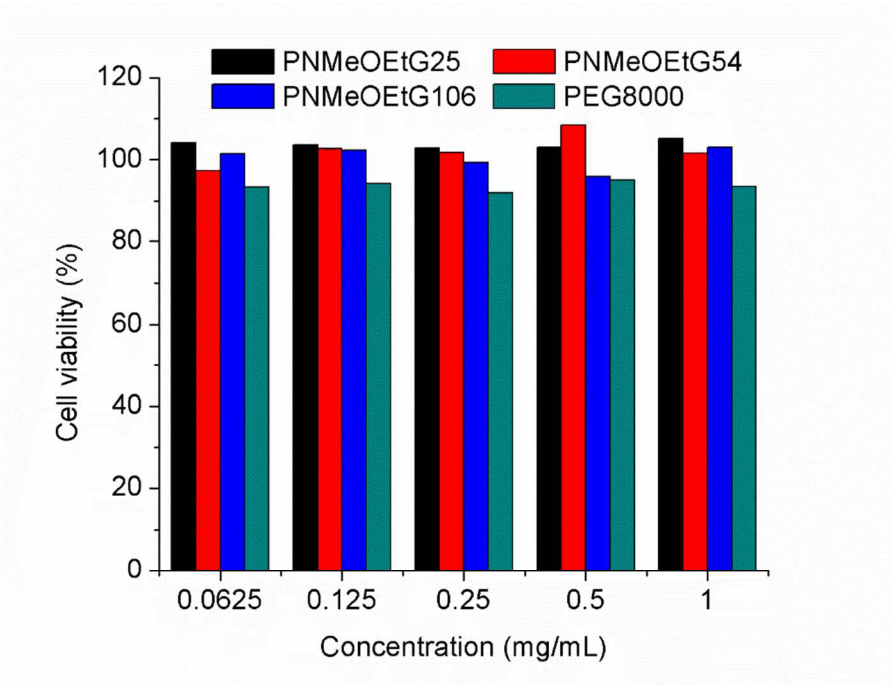

Figure 10. Cell viability study of PNMeOEtG polypeptoids compared to PEG (8000 Da). The DP_ns listed in the figure were determined from NMR end-group analysis. The error bars in the figure are the standard deviations of three measurements.

Conclusions. *N* substituted *N*-carboxyanhydride monomers bearing oligomeric ethylene glycol side chains $(Me(OEt)_n$-NCA (n = 1-3) have been successfully synthesized in good yields. Polymerization of $(Me(OEt)_n$-NCA (n = 1-3) monomers using primary amine initiators proceeds in a controlled manner, yielding the corresponding PEGylated polypeptoids ($PNMe(OEt)_nG$, n = 1-3) having well-defined structures with controlled molecular weight in the 3.26-28.6 kg/mol range and narrow molecular distribution (PDI = 1.03-1.10). The resulting PEGylated polypeptoids are amorphous with glass transition temperatures decreasing with increased oligomeric ethylene glycol sidechain length. The PNMeOEtG polymers are highly water soluble (solubility > 200 mg/mL at room temperature) and are minimally cytotoxic towards Hep2 cells. DLS And SANS analysis of the aqueous solution containing a mixture of PNMeOEtG and

lysozyme at 1 wt% concentration revealed minimal interactions between lysozyme and PNMeOEtG in water, underscoring the potential of the PEGylated polypeptoids as promising anti-fouling materials for biomedical and biotechnological applications.

Supporting Information:

^{1}H and $^{13}C\{^{1}H\}$ spectra for precursor of monomers, monomers and corresponding PEGylated polypeptoids, SEC-DRI chromatograms of PEGylated polypeptoids, MALDI-TOF MS spectra of PEGylated polypeptoids, TGA and DSC graphs of PEGylated polypeptoids, DLS analysis of 1 wt% PNMeOEtG106 in PBS, DLS analysis of 1 wt% lysozyme in PBS, DLS analysis of 1 wt% PEG8000 in PBS, DLS of the mixture of 1 wt% PEG8000 and 1 wt% lysozyme in PBS, SEC chromatograms and M_n and PDI data from polymerization of MeOEt-NCA in toluene. This material is available free of charge via the Internet at http://pubs.acs.org

Corresponding Author

Email: dhzhang@lsu.edu and gjschneider@lsu.edu

Notes

The author declare no competing financial interest.

Acknowledgments

We would like to acknowledge Dr. Rafael Cueto for his assistance with the TGA measurements. This work is supported by the National Science Foundation (CHE 0955820 and CHE 1609447) and the Louisiana State University. The neutron scattering work conducted by SG is supported by the U.S. Department of Energy under EPSCoR Grant No. DE-SC0012432 with additional support from the Louisiana Board of Regents. This work utilized facilities were supported in part by the National Science Foundation under Agreement No. DMR-1508249. We

acknowledge the support of the National Institute of Standards and Technology (NIST), U.S. Department of Commerce, in providing the neutron research facilities used in this work.

References

1. Meyers, S. R.; Grinstaff, M. W. Biocompatible and Bioactive Surface Modifications for Prolonged in Vivo Efficacy. *Chem. Rev.* **2012,** *112* (3), 1615-1632.
2. Horbett, T. A., Protein Adsorption on Biomaterials. In *Biomaterials: Interfacial Phenomena and Applications*, American Chemical Society: 1982; Vol. 199, pp 233-244.
3. Mojtaba, B.; Maryam, K.; Larry, D. U., Poly(Ethylene Glycol) and Poly(Carboxy Betaine) Based Nonfouling Architectures: Review and Current Efforts. In *Proteins at Interfaces Iii State of the Art*, American Chemical Society: 2012; Vol. 1120, pp 621-643.
4. Wei, Q.; Becherer, T.; Angioletti-Uberti, S.; Dzubiella, J.; Wischke, C.; Neffe, A. T.; Lendlein, A.; Ballauff, M.; Haag, R. Protein Interactions with Polymer Coatings and Biomaterials. *Angew. Chem. Int. Ed.* **2014,** *53* (31), 8004-8031.
5. Pertsin, A. J.; Grunze, M. Computer Simulation of Water near the Surface of Oligo(Ethylene Glycol)-Terminated Alkanethiol Self-Assembled Monolayers. *Langmuir* **2000,** *16* (23), 8829-8841.
6. Chapman, R. G.; Ostuni, E.; Takayama, S.; Holmlin, R. E.; Yan, L.; Whitesides, G. M. Surveying for Surfaces That Resist the Adsorption of Proteins. *J. Am. Chem. Soc.* **2000,** *122* (34), 8303-8304.
7. Ostuni, E.; Chapman, R. G.; Holmlin, R. E.; Takayama, S.; Whitesides, G. M. A Survey of Structure−Property Relationships of Surfaces That Resist the Adsorption of Protein. *Langmuir* **2001,** *17* (18), 5605-5620.
8. Knop, K.; Hoogenboom, R.; Fischer, D.; Schubert, U. S. Poly(Ethylene Glycol) in Drug Delivery: Pros and Cons as Well as Potential Alternatives. *Angew. Chem. Int. Ed.* **2010,** *49* (36), 6288-6308.
9. Romberg, B.; Metselaar, J. M.; Baranyi, L.; Snel, C. J.; Bünger, R.; Hennink, W. E.; Szebeni, J.; Storm, G. Poly(Amino Acid)S: Promising Enzymatically Degradable Stealth Coatings for Liposomes. *Int. J. Pharm.* **2007,** *331* (2), 186-189.
10. Chelmowski, R.; Köster, S. D.; Kerstan, A.; Prekelt, A.; Grunwald, C.; Winkler, T.; Metzler-Nolte, N.; Terfort, A.; Wöll, C. Peptide-Based Sams That Resist the Adsorption of Proteins. *J. Am. Chem. Soc.* **2008,** *130* (45), 14952-14953.
11. Engler, A. C.; Ke, X.; Gao, S.; Chan, J. M. W.; Coady, D. J.; Ono, R. J.; Lubbers, R.; Nelson, A.; Yang, Y. Y.; Hedrick, J. L. Hydrophilic Polycarbonates: Promising Degradable Alternatives to Poly(Ethylene Glycol)-Based Stealth Materials. *Macromolecules* **2015,** *48* (6), 1673-1678.
12. Konradi, R.; Pidhatika, B.; Mühlebach, A.; Textor, M. Poly-2-Methyl-2-Oxazoline: A Peptide-Like Polymer for Protein-Repellent Surfaces. *Langmuir* **2008,** *24* (3), 613-616.
13. Pidhatika, B.; Möller, J.; Benetti, E. M.; Konradi, R.; Rakhmatullina, E.; Mühlebach, A.; Zimmermann, R.; Werner, C.; Vogel, V.; Textor, M. The Role of the Interplay between Polymer

Architecture and Bacterial Surface Properties on the Microbial Adhesion to Polyoxazoline-Based Ultrathin Films. *Biomaterials* **2010,** *31* (36), 9462-9472.
14. Hoogenboom, R. Poly(2-Oxazoline)S: A Polymer Class with Numerous Potential Applications. *Angew. Chem. Int. Ed.* **2009,** *48* (43), 7978-7994.
15. Teare, D. O. H.; Schofield, W. C. E.; Garrod, R. P.; Badyal, J. P. S. Poly(N-Acryloylsarcosine Methyl Ester) Protein-Resistant Surfaces. *J. Phys. Chem. B* **2005,** *109* (44), 20923-20928.
16. Huber, D. L.; Manginell, R. P.; Samara, M. A.; Kim, B.-I.; Bunker, B. C. Programmed Adsorption and Release of Proteins in a Microfluidic Device. *Science* **2003,** *301* (5631), 352-354.
17. Yang, J.; Zhang, M.; Chen, H.; Chang, Y.; Chen, Z.; Zheng, J. Probing the Structural Dependence of Carbon Space Lengths of Poly(N-Hydroxyalkyl Acrylamide)-Based Brushes on Antifouling Performance. *Biomacromolecules* **2014,** *15* (8), 2982-2991.
18. Chan, J. M. W.; Ke, X.; Sardon, H.; Engler, A. C.; Yang, Y. Y.; Hedrick, J. L. Chemically Modifiable N-Heterocycle-Functionalized Polycarbonates as a Platform for Diverse Smart Biomimetic Nanomaterials. *Chem. Sci.* **2014,** *5* (8), 3294-3300.
19. Yang, W.; Sundaram, H. S.; Ella, J.-R.; He, N.; Jiang, S. Low-Fouling Electrospun Plla Films Modified with Zwitterionic Poly(Sulfobetaine Methacrylate)-Catechol Conjugates. *Acta Biomater.* **2016,** *40*, 92-99.
20. Jeong, J. H.; Song, S. H.; Lim, D. W.; Lee, H.; Park, T. G. DNA Transfection Using Linear Poly(Ethylenimine) Prepared by Controlled Acid Hydrolysis of Poly(2-Ethyl-2-Oxazoline). *J. Controlled Release* **2001,** *73* (2–3), 391-399.
21. Wang, C.-H.; Fan, K.-R.; Hsiue, G.-H. Enzymatic Degradation of Plla-Peoz-Plla Triblock Copolymers. *Biomaterials* **2005,** *26* (16), 2803-2811.
22. Duracher, D.; Veyret, R.; Elaïssari, A.; Pichot, C. Adsorption of Bovine Serum Albumin Protein onto Amino-Containing Thermosensitive Core-Shell Latexes. *Polym. Int.* **2004,** *53* (5), 618-626.
23. Miller, S. M.; Simon, R. J.; Ng, S.; Zuckermann, R. N.; Kerr, J. M.; Moos, W. H. Proteolytic Studies of Homologous Peptide and N-Substituted Glycine Peptoid Oligomers. *Biorg. Med. Chem. Lett.* **1994,** *4* (22), 2657-2662.
24. Miller, S. M.; Simon, R. J.; Ng, S.; Zuckermann, R. N.; Kerr, J. M.; Moos, W. H. Comparison of the Proteolytic Susceptibilities of Homologous L-Amino Acid, D-Amino Acid, and N-Substituted Glycine Peptide and Peptoid Oligomers. *Drug Dev. Res.* **1995,** *35* (1), 20-32.
25. Patch, J. A.; Barron, A. E. Mimicry of Bioactive Peptides Via Non-Natural, Sequence-Specific Peptidomimetic Oligomers. *Curr. Opin. Chem. Biol.* **2002,** *6* (6), 872-877.
26. Latham, P. W. Therapeutic Peptides Revisited. *Nat. Biotechnol.* **1999,** *17* (8), 755-757.
27. Hardesty, J. O.; Cascão-Pereira, L.; Kellis, J. T.; Robertson, C. R.; Frank, C. W. Enzymatic Proteolysis of a Surface-Bound A-Helical Polypeptide. *Langmuir* **2008,** *24* (24), 13944-13956.
28. De Marre, A.; Hoste, K.; Bruneel, D.; Schacht, E.; De Schryver, F. Synthesis, Characterization, and in Vitro Biodegradation of Poly(Ethylene Glycol) Modified Poly[5n-(2-Hydroxyethyl-L-Glutamine]. *J. Bioact. Compatible Polym.* **1996,** *11* (2), 85-99.
29. Gabizon, A. P., D. Liposome Formulations with Prolonged Circulation Time in Blood and Enhanced Uptake by Tumors. *Proc. Natl. Acad. Sci. U.S.A.* **1988,** *85* (18), 6949-6953.
30. Friend, D. R.; Pangburn, S. Site-Specific Drug Delivery. *Med. Res. Rev.* **1987,** *7* (1), 53-106.

31. Tempelaar, S.; Mespouille, L.; Coulembier, O.; Dubois, P.; Dove, A. P. Synthesis and Post-Polymerisation Modifications of Aliphatic Poly(Carbonate)S Prepared by Ring-Opening Polymerisation. *Chem. Soc. Rev.* **2013,** *42* (3), 1312-1336.
32. Pascual, A.; Tan, J. P. K.; Yuen, A.; Chan, J. M. W.; Coady, D. J.; Mecerreyes, D.; Hedrick, J. L.; Yang, Y. Y.; Sardon, H. Broad-Spectrum Antimicrobial Polycarbonate Hydrogels with Fast Degradability. *Biomacromolecules* **2015,** *16* (4), 1169-1178.
33. Wang, H.-F.; Su, W.; Zhang, C.; Luo, X.-h.; Feng, J. Biocatalytic Fabrication of Fast-Degradable, Water-Soluble Polycarbonate Functionalized with Tertiary Amine Groups in Backbone. *Biomacromolecules* **2010,** *11* (10), 2550-2557.
34. Zhang, Z.; Kuijer, R.; Bulstra, S. K.; Grijpma, D. W.; Feijen, J. The in Vivo and in Vitro Degradation Behavior of Poly(Trimethylene Carbonate). *Biomaterials* **2006,** *27* (9), 1741-1748.
35. Zhang, D.; Lahasky, S. H.; Guo, L.; Lee, C.-U.; Lavan, M. Polypeptoid Materials: Current Status and Future Perspectives. *Macromolecules* **2012,** *45* (15), 5833-5841.
36. Barron, A. E.; Zuckerman, R. N. Bioinspired Polymeric Materials: In-between Proteins and Plastics. *Curr. Opin. Chem. Biol.* **1999,** *3* (6), 681-687.
37. Lahasky, S. H.; Hu, X.; Zhang, D. Thermoresponsive Poly(A-Peptoid)S: Tuning the Cloud Point Temperatures by Composition and Architecture. *ACS Macro Letters* **2012,** *1* (5), 580-584.
38. Fetsch, C.; Flecks, S.; Gieseler, D.; Marschelke, C.; Ulbricht, J.; van Pée, K.-H.; Luxenhofer, R. Self-Assembly of Amphiphilic Block Copolypeptoids with C2-C5 Side Chains in Aqueous Solution. *Macromol. Chem. Phys.* **2015,** *216* (5), 547-560.
39. Xuan, S.; Lee, C.-U.; Chen, C.; Doyle, A. B.; Zhang, Y.; Guo, L.; John, V. T.; Hayes, D.; Zhang, D. Thermoreversible and Injectable Abc Polypeptoid Hydrogels: Controlling the Hydrogel Properties through Molecular Design. *Chem. Mater.* **2016,** *28* (3), 727-737.
40. Li, A.; Zhang, D. Synthesis and Characterization of Cleavable Core-Cross-Linked Micelles Based on Amphiphilic Block Copolypeptoids as Smart Drug Carriers. *Biomacromolecules* **2016,** *17* (3), 852-861.
41. Ulbricht, J.; Jordan, R.; Luxenhofer, R. On the Biodegradability of Polyethylene Glycol, Polypeptoids and Poly(2-Oxazoline)S. *Biomaterials* **2014,** *35* (17), 4848-4861.
42. Sun, J.; Zuckermann, R. N. Peptoid Polymers: A Highly Designable Bioinspired Material. *ACS Nano* **2013,** *7* (6), 4715-4732.
43. Luxenhofer, R.; Fetsch, C.; Grossmann, A. Polypeptoids: A Perfect Match for Molecular Definition and Macromolecular Engineering? *J. Polym. Sci., Part A: Polym. Chem.* **2013,** *51* (13), 2731-2752.
44. Zuckermann, R. N. Peptoid Origins. *Pep. Sci.* **2011,** *96* (5), 545-555.
45. Secker, C.; Brosnan, S. M.; Luxenhofer, R.; Schlaad, H. Poly(A-Peptoid)S Revisited: Synthesis, Properties, and Use as Biomaterial. *Macromol. Biosci.* **2015,** *15* (7), 881-891.
46. Lau, K. H. A.; Ren, C.; Sileika, T. S.; Park, S. H.; Szleifer, I.; Messersmith, P. B. Surface-Grafted Polysarcosine as a Peptoid Antifouling Polymer Brush. *Langmuir* **2012,** *28* (46), 16099-16107.
47. Lau, K. H. A.; Ren, C.; Park, S. H.; Szleifer, I.; Messersmith, P. B. An Experimental–Theoretical Analysis of Protein Adsorption on Peptidomimetic Polymer Brushes. *Langmuir* **2011,** *28* (4), 2288-2298.
48. Statz, A. R.; Barron, A. E.; Messersmith, P. B. Protein, Cell and Bacterial Fouling Resistance of Polypeptoid-Modified Surfaces: Effect of Side-Chain Chemistry. *Soft Matter* **2008,** *4* (1), 131-139.

49. Schneider, M.; Fetsch, C.; Amin, I.; Jordan, R.; Luxenhofer, R. Polypeptoid Brushes by Surface-Initiated Polymerization of N-Substituted Glycine N-Carboxyanhydrides. *Langmuir* **2013,** *29* (23), 6983-6988.
50. Sun, J.; Stone, G. M.; Balsara, N. P.; Zuckermann, R. N. Structure–Conductivity Relationship for Peptoid-Based Peo–Mimetic Polymer Electrolytes. *Macromolecules* **2012,** *45* (12), 5151-5156.
51. Frisken, B. J. Revisiting the Method of Cumulants for the Analysis of Dynamic Light-Scattering Data. *Appl. Opt.* **2001,** *40* (24), 4087-4091.
52. Gupta, S.; Camargo, M.; Stellbrink, J.; Allgaier, J.; Radulescu, A.; Lindner, P.; Zaccarelli, E.; Likos, C. N.; Richter, D. Dynamic Phase Diagram of Soft Nanocolloids. *Nanoscale* **2015,** *7* (33), 13924-13934.
53. Kinning, D. J.; Thomas, E. L. Hard-Sphere Interactions between Spherical Domains in Diblock Copolymers. *Macromolecules* **1984,** *17* (9), 1712-1718.
54. Percus, J. K.; Yevick, G. J. Analysis of Classical Statistical Mechanics by Means of Collective Coordinates. *Phys. Rev.* **1958,** *110* (1), 1-13.
55. Debye, P. Molecular-Weight Determination by Light Scattering. *J. Phys. Colloid. Chem.* **1947,** *51* (1), 18-32.
56. Xuan, S.; Zhao, N.; Zhou, Z.; Fronczek, F. R.; Vicente, M. G. H. Synthesis and in Vitro Studies of a Series of Carborane-Containing Boron Dipyrromethenes (Bodipys). *J. Med. Chem.* **2016,** *59* (5), 2109-2117.
57. Robinson, J. W.; Secker, C.; Weidner, S.; Schlaad, H. Thermoresponsive Poly(N-C3 Glycine)S. *Macromolecules* **2013,** *46* (3), 580-587.
58. Guo, L.; Zhang, D. Cyclic Poly(A-Peptoid)S and Their Block Copolymers from N-Heterocyclic Carbene-Mediated Ring-Opening Polymerizations of N-Substituted N-Carboxylanhydrides. *J. Am. Chem. Soc.* **2009,** *131* (50), 18072-18074.
59. Arbe, A.; Genix, A. C.; Colmenero, J.; Richter, D.; Fouquet, P. Anomalous Relaxation of Self-Assembled Alkyl Nanodomains in High-Order Poly(N-Alkyl Methacrylates). *Soft Matter* **2008,** *4* (9), 1792-1795.
60. Gerstl, C.; Schneider, G. J.; Fuxman, A.; Zamponi, M.; Frick, B.; Seydel, T.; Koza, M.; Genix, A. C.; Allgaier, J.; Richter, D.; Colmenero, J.; Arbe, A. Quasielastic Neutron Scattering Study on the Dynamics of Poly(Alkylene Oxide)S. *Macromolecules* **2012,** *45* (10), 4394-4405.
61. Moreno, A. J.; Arbe, A.; Colmenero, J. Structure and Dynamics of Self-Assembled Comb Copolymers: Comparison between Simulations of a Generic Model and Neutron Scattering Experiments. *Macromolecules* **2011,** *44* (6), 1695-1706.
62. Arbe, A.; Genix, A. C.; Arrese-Igor, S.; Colmenero, J.; Richter, D. Dynamics in Poly(N-Alkyl Methacrylates): A Neutron Scattering, Calorimetric, and Dielectric Study. *Macromolecules* **2010,** *43* (6), 3107-3119.
63. Gerstl, C.; Schneider, G. J.; Pyckhout-Hintzen, W.; Allgaier, J.; Richter, D.; Alegría, A.; Colmenero, J. Segmental and Normal Mode Relaxation of Poly(Alkylene Oxide)S Studied by Dielectric Spectroscopy and Rheology. *Macromolecules* **2010,** *43* (11), 4968-4977.
64. Fetsch, C.; Luxenhofer, R. Thermal Properties of Aliphatic Polypeptoids. *Polymers* **2013,** *5* (1), 112.
65. Biswas, C. S.; Patel, V. K.; Vishwakarma, N. K.; Tiwari, V. K.; Maiti, B.; Maiti, P.; Kamigaito, M.; Okamoto, Y.; Ray, B. Effects of Tacticity and Molecular Weight of Poly(N-Isopropylacrylamide) on Its Glass Transition Temperature. *Macromolecules* **2011,** *44* (14), 5822-5824.

66. Gupta, S.; Fischer, J. K. H.; Lunkenheimer, P.; Loidl, A.; Novak, E.; Jalarvo, N.; Ohl, M. Effect of Adding Nanometre-Sized Heterogeneities on the Structural Dynamics and the Excess Wing of a Molecular Glass Former. *Sci. Rep.* **2016,** *6*, 35034.
67. Stradner, A.; Sedgwick, H.; Cardinaux, F.; Poon, W. C. K.; Egelhaaf, S. U.; Schurtenberger, P. Equilibrium Cluster Formation in Concentrated Protein Solutions and Colloids. *Nature* **2004,** *432* (7016), 492-495.
68. Diamond, R. Real-Space Refinement of the Structure of Hen Egg-White Lysozyme. *J. Mol. Biol.* **1974,** *82* (3), 371-391.
69. Shukla, A.; Mylonas, E.; Di Cola, E.; Finet, S.; Timmins, P.; Narayanan, T.; Svergun, D. I. Absence of Equilibrium Cluster Phase in Concentrated Lysozyme Solutions. *Proc. Natl. Acad. Sci.* **2008,** *105* (13), 5075-5080.
70. Narayanan, J.; Liu, X. Y. Protein Interactions in Undersaturated and Supersaturated Solutions: A Study Using Light and X-Ray Scattering. *Biophys. J.* **2003,** *84* (1), 523-532.
71. Tanford, C.; Roxby, R. Interpretation of Protein Titration Curves. Application to Lysozyme. *Biochemistry* **1972,** *11* (11), 2192-2198.
72. Gupta, S.; Biehl, R.; Sill, C.; Allgaier, J.; Sharp, M.; Ohl, M.; Richter, D. Protein Entrapment in Polymeric Mesh: Diffusion in Crowded Environment with Fast Process on Short Scales. *Macromolecules* **2016,** *49* (5), 1941-1949.

Well-defined PEGylated polypeptoids as protein-resistant polymers

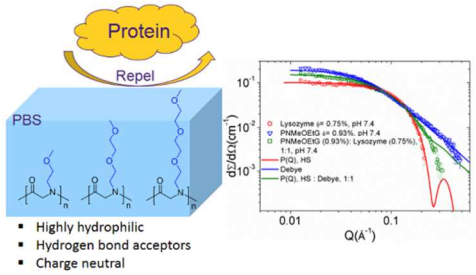

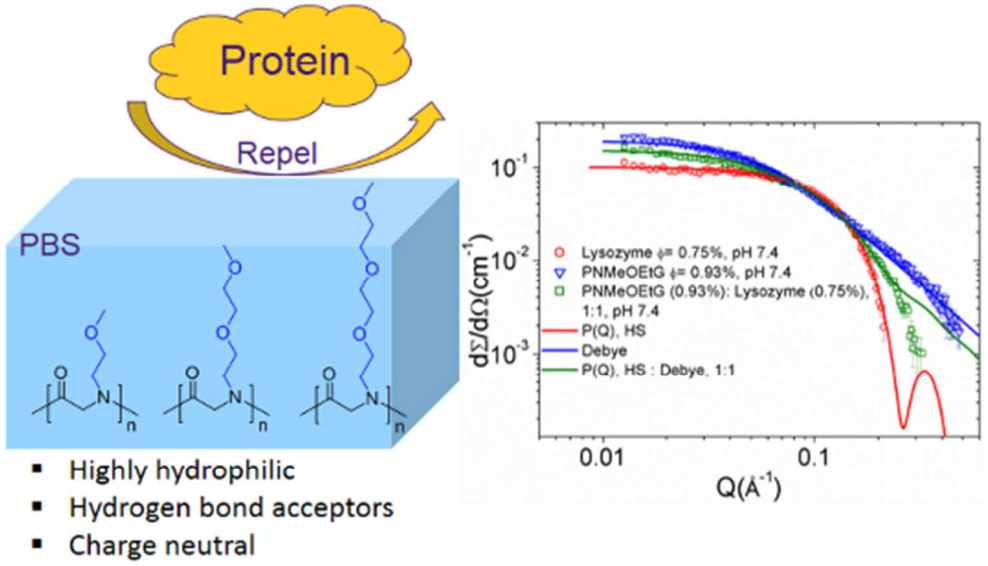

Synthesis and Characterization of Well-defined PEGylated Polypeptoids as Protein-resistant Polymers† Sunting Xuan, Sudipta Gupta, Xin Li, Markus Bleuel, Gerald J. Schneider and Donghui Zhang*

63x35mm (220 x 220 DPI)